mortality (and probably morbidity) reductions linked to measles vaccination might be much greater than previously considered. This is of particular importance today where, especially in wealthy nations, reduced opportunistic infections during acute measles immunosuppression, added to the comparative rarity of infection, has led to a public view of measles as a benign childhood disease. Our findings help dispel the mystery surrounding the disproportionately large reductions in mortality seen after the introduction of measles vaccinations and reinforce the importance of measles vaccination in a global context.

REFERENCES AND NOTES

1. W. J. Moss, D. E. Griffin, *Lancet* **379**, 153–164 (2012).
2. E. Simons *et al.*, *Lancet* **379**, 2173–2178 (2012).
3. R. T. Perry *et al.*, *MMWR Morb. Mortal. Wkly. Rep.* **63**, 103–107 (2014).
4. S. B. Omer, D. A. Salmon, W. A. Orenstein, M. P. deHart, N. Halsey, *N. Engl. J. Med.* **360**, 1981–1988 (2009).
5. J. D. Clemens *et al.*, *Am. J. Epidemiol.* **128**, 1330–1339 (1988).
6. M. A. Koenig *et al.*, *Bull. World Health Organ.* **68**, 441–447 (1990).
7. A. Desgrées du Loû, G. Pison, P. Aaby, *Am. J. Epidemiol.* **142**, 643–652 (1995).
8. P. Aaby, J. Bukh, I. M. Lisse, A. J. Smits, *J. Infect.* **8**, 13–21 (1984).
9. E. A. Holt, R. Boulos, N. A. Halsey, L. M. Boulos, C. Boulos, *Pediatrics* **85**, 188–194 (1990).
10. Z. Kabir, J. Long, V. P. Reddaiah, J. Kevany, S. K. Kapoor, *Bull. World Health Organ.* **81**, 244–250 (2003).
11. P. Aaby, T. R. Kollmann, C. S. Benn, *Nat. Immunol.* **15**, 895–899 (2014).
12. P. Aaby *et al.*, *Int. J. Epidemiol.* **32**, 106–115 (2003).
13. K. L. Flanagan *et al.*, *Clin. Infect. Dis.* **57**, 283–289 (2013).
14. C. L. Karp *et al.*, *Science* **273**, 228–231 (1996).
15. B. Hahm, *Curr. Top. Microbiol. Immunol.* **330**, 271–287 (2009).
16. S. Schneider-Schaulies, J. Schneider-Schaulies, *Curr. Top. Microbiol. Immunol.* **330**, 243–269 (2009).
17. R. D. de Vries *et al.*, *PLOS Pathog.* **8**, e1002885 (2012).
18. J. Kleinnijenhuis *et al.*, *Proc. Natl. Acad. Sci. U.S.A.* **109**, 17537–17542 (2012).
19. G. R. Lee, S. T. Kim, C. G. Spilianakis, P. E. Fields, R. A. Flavell, *Immunity* **24**, 369–379 (2006).
20. M. G. Netea, J. Quintin, J. W. van der Meer, *Cell Host Microbe* **9**, 355–361 (2011).
21. S. Saeed *et al.*, *Science* **345**, 1251086 (2014).
22. WHO, Meeting of the Strategic Advisory Group of Experts on immunization, March 2014, *Systematic Review of the Non-specific Effects of BCG, DTP and Measles Containing Vaccines*, http://www.who.int/immunization/sage/meetings/2014/april/3_NSE_Epidemiology_review_Report_to_SAGE_14_Mar_FINAL.pdf.
23. R. D. de Vries, R. L. de Swart, *PLOS Pathog.* **10**, e1004482 (2014).
24. W. H. Lin, R. D. Kouyos, R. J. Adams, B. T. Grenfell, D. E. Griffin, *Proc. Natl. Acad. Sci. U.S.A.* **109**, 14989–14994 (2012).
25. R. T. Perry, N. A. Halsey, *J. Infect. Dis.* **189**, S4–S16 (2004).
26. L. K. Selin, K. Vergilis, R. M. Welsh, S. R. Nahill, *J. Exp. Med.* **183**, 2489–2499 (1996).
27. S. K. Kim, M. A. Brehm, R. M. Welsh, L. K. Selin, *J. Immunol.* **169**, 90–98 (2002).
28. S. K. Kim, R. M. Welsh, *J. Immunol.* **172**, 3139–3150 (2004).
29. C. D. Peacock, S. K. Kim, R. M. Welsh, *J. Immunol.* **171**, 655–663 (2003).
30. A. R. Hinman, W. A. Orenstein, M. J. Papania, *J. Infect. Dis.* **189**, S17–S22 (2004).
31. P. Aaby, J. Bukh, D. Kronborg, I. M. Lisse, M. C. da Silva, *Am. J. Epidemiol.* **132**, 211–219 (1990).
32. WHO, *Global Review of the Distribution of Pneumococcal Invasive Disease by Age and Region* (2011); www.who.int/immunization/sage/6_Russel_review_age_specific_epidemiology_PCV_schedules_session_nov11.pdf.
33. O. Horwitz, K. Grünfeld, B. Lysgaard-Hansen, K. Kjeldsen, *Am. J. Epidemiol.* **100**, 136–149 (1974).
34. J. A. Clarkson, P. E. M. Fine, *Int. J. Epidemiol.* **14**, 153–168 (1985).
35. A. Kipps, L. Stern, E. Vaughan, *S. Afr. Med. J.* **86**, 104–108 (1996).
36. S. O. Shaheen *et al.*, *BMJ* **313**, 969–974 (1996).
37. S. O. Shaheen *et al.*, *Lancet* **347**, 1792–1796 (1996).
38. P. Aaby, B. Samb, M. Andersen, F. Simondon, *Am. J. Epidemiol.* **143**, 1035–1041 (1996).
39. P. Aaby, I. M. Lisse, K. Mølbak, K. Knudsen, H. Whittle, *Pediatr. Infect. Dis. J.* **15**, 39–44 (1996).
40. D. J. Earn, P. Rohani, B. M. Bolker, B. T. Grenfell, *Science* **287**, 667–670 (2000).

ACKNOWLEDGMENTS

Data for analyses regarding England and Wales were retrieved from the Office of Population Censuses and Surveys and the Office for National Statistics (www.ons.gov.uk). We thank P. Rohani for supplying us with historical data on pertussis, as originally described in (*34*). Data for U.S. analyses were retrieved from the U.S. Centers for Disease Control and Prevention, National Center for Health Statistics (www.cdc.gov/nchs). Data for Denmark was retrieved from Statistics Denmark (www.statbank.dk) and WHO (www.apps.who.int). This work is funded by the Bill and Melinda Gates Foundation, the Science and Technology Directorate of the Department of Homeland Security [contract HSHQDC-12-C-00058 (B.T.G. and C.J.E.M.)], and the RAPIDD program of the Science and Technology Directorate of the Department of Homeland Security and the Fogarty International Center, National Institutes of Health (C.J.E.M. and B.T.G).

SUPPLEMENTARY MATERIALS

www.sciencemag.org/content/348/6235/694/suppl/DC1
Materials and Methods
Supplementary Text
Figs. S1 to S13
Table S1
References (*41*–*43*)
Movies S1 to S3

24 November 2014; accepted 1 April 2015
10.1126/science.aaa3662

CHROMOSOMES

CENP-C reshapes and stabilizes CENP-A nucleosomes at the centromere

Samantha J. Falk,[1,2]* Lucie Y. Guo,[1,3]* Nikolina Sekulic,[1]* Evan M. Smoak,[1,3,4]* Tomoyasu Mani,[1,3] Glennis A. Logsdon,[1,3] Kushol Gupta,[1] Lars E. T. Jansen,[5] Gregory D. Van Duyne,[1,3] Sergei A. Vinogradov,[1,3] Michael A. Lampson,[2,3,4] Ben E. Black[1,2,3]†

Inheritance of each chromosome depends upon its centromere. A histone H3 variant, centromere protein A (CENP-A), is essential for epigenetically marking centromere location. We find that CENP-A is quantitatively retained at the centromere upon which it is initially assembled. CENP-C binds to CENP-A nucleosomes and is a prime candidate to stabilize centromeric chromatin. Using purified components, we find that CENP-C reshapes the octameric histone core of CENP-A nucleosomes, rigidifies both surface and internal nucleosome structure, and modulates terminal DNA to match the loose wrap that is found on native CENP-A nucleosomes at functional human centromeres. Thus, CENP-C affects nucleosome shape and dynamics in a manner analogous to allosteric regulation of enzymes. CENP-C depletion leads to rapid removal of CENP-A from centromeres, indicating their collaboration in maintaining centromere identity.

Centromeres direct chromosome inheritance at cell division, and nucleosomes containing a histone H3 variant, centromere protein A (CENP-A), are central to current models of an epigenetic program for specifying centromere location (*1*). The centromere inheritance model in metazoans suggests that the high local concentration of preexisting CENP-A nucleosomes at the centromere guides the assembly of nascent CENP-A, which occurs once per cell cycle after mitotic exit. This model predicts that after initial assembly into centromeric chromatin, CENP-A must be stably retained at that centromere; otherwise, centromere identity would be lost before the next opportunity for new loading in the next cell cycle. Here, we use biochemical reconstitution to measure the shape and physical properties of CENP-A nucleosomes with and without its close binding partner, CENP-C, and combine these studies with functional tests that reveal the mechanisms underlying the high stability of centromeric chromatin.

CENP-C recognizes CENP-A nucleosomes via a region termed its central domain (amino acids 426 to 537; CENP-C^{CD}) (*2*, *3*). We first considered how CENP-C^{CD} may affect the overall shape of the CENP-A–containing nucleosome using an intranucleosomal fluorescence resonance energy transfer (FRET)–based approach. We designed an experiment to measure FRET efficiency, Φ_{FRET},

[1]Department of Biochemistry and Biophysics, Perelman School of Medicine, University of Pennsylvania, Philadelphia, PA 19104, USA. [2]Graduate Program in Cell and Molecular Biology, Perelman School of Medicine, University of Pennsylvania, Philadelphia, PA 19104, USA. [3]Graduate Program in Biochemistry and Molecular Biophysics, Perelman School of Medicine, University of Pennsylvania, Philadelphia, PA 19104, USA. [4]Department of Biology, University of Pennsylvania, Philadelphia, PA 19104, USA. [5]Instituto Gulbenkian de Ciência, 2780-156 Oeiras, Portugal.
*These authors contributed equally to this work. **†Corresponding author. E-mail: blackbe@mail.med.upenn.edu**

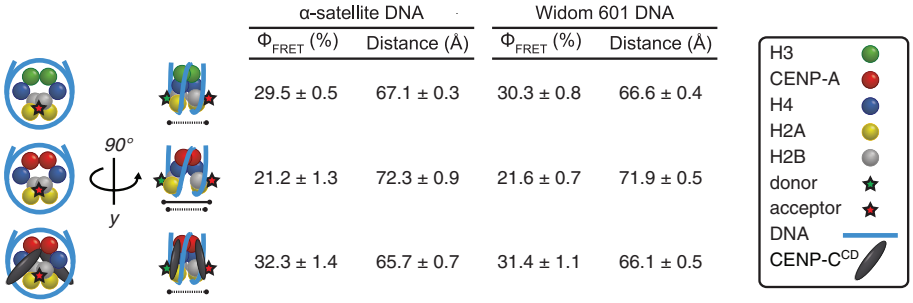

	α-satellite DNA		Widom 601 DNA	
	Φ_{FRET} (%)	Distance (Å)	Φ_{FRET} (%)	Distance (Å)
	29.5 ± 0.5	67.1 ± 0.3	30.3 ± 0.8	66.6 ± 0.4
	21.2 ± 1.3	72.3 ± 0.9	21.6 ± 0.7	71.9 ± 0.5
	32.3 ± 1.4	65.7 ± 0.7	31.4 ± 1.1	66.1 ± 0.5

Fig. 1. CENP-A nucleosomes have a conventional shape only upon CENP-C^{CD} binding. Calculated FRET efficiencies (Φ_{FRET}) and distances between donor and acceptor fluorophores on H2B S123C for the indicated nucleosomes on either α-satellite or Widom 601 DNA. Data are shown as the mean ± SEM of three independent nucleosome reconstitutions.

between two fluorophores on defined positions on the H2B subunits of CENP-A nucleosomes in the absence or presence of CENP-C^{CD} and then used these measurements to calculate intranucleosomal distances (Fig. 1 and fig. S1). The H2B distances for CENP-A nucleosomes in the absence of CENP-C^{CD} are ~5 Å farther apart than expected from their crystal structure (PDB ID 3AN2) (*4*), indicating that CENP-A–containing nucleosomes in solution prefer a histone octamer configuration not captured in the crystal structure. It is likely that CENP-A nucleosomes sample both conformations in solution, with crystal contacts stabilizing the form that was reported (*4*). In contrast to CENP-A nucleosomes, conventional

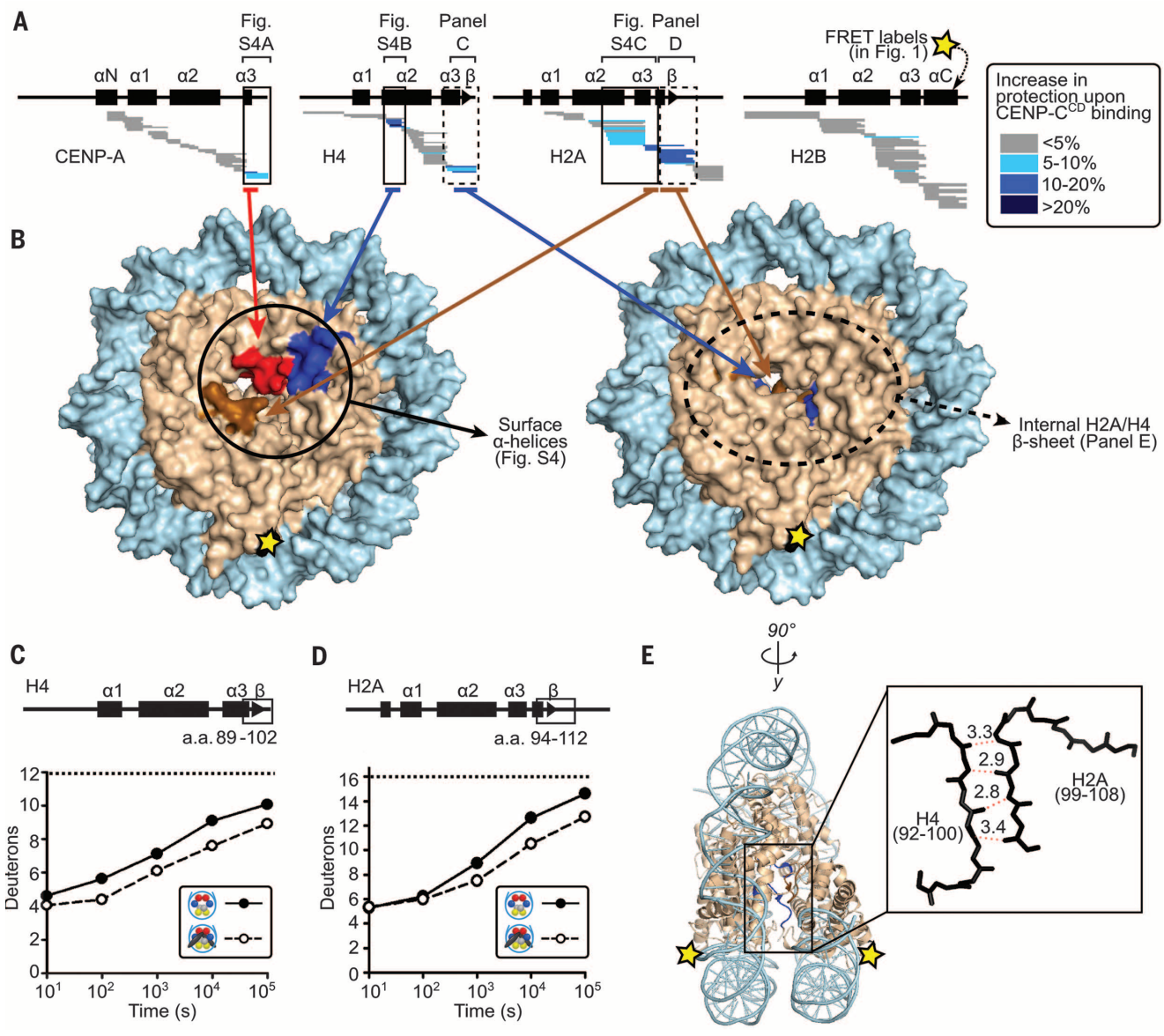

Fig. 2. CENP-C^{CD} rigidifies CENP-A nucleosomes. (**A**) HXMS of all histone subunits of the CENP-A nucleosome from a single time point (10^4 s; see all time points in fig. S3). Each horizontal bar represents an individual peptide, and peptides are placed beneath schematics of secondary structural elements. (**B**) Regions showing substantial protection from HX mapped onto the structure of the CENP-A nucleosome (PDB ID 3AN2). (**C** and **D**) Comparison of representative peptides spanning the β-sheet region in histone H4 and histone H2A over the time course. The maximum number of deuterons possible to measure by HXMS for each peptide is shown by the dotted line. (**E**) The internal H4/H2A interface mapped (see fig. S5) onto the canonical nucleosome crystal structure (PDB ID 1KX5).

nucleosomes have smaller H2B distances in solution (Fig. 1) that are consistent with their crystal structure (*5*). Separation of H2A/H2B dimers from each other is consistent with a nucleosome model based on rotation of the CENP-A/CENP-A′ interface in $(CENP\text{-}A/H4)_2$ heterotetramers (*6*). Upon binding of CENP-C^{CD}, with the known stoichiometry of two CENP-C^{CD} molecules per nucleosome (*3*), the H2A/H2B distances shorten to ones that are nearly identical to those in conventional nucleosomes (Fig. 1). The differences we observed between H3 nucleosomes, CENP-A nucleosomes, and CENP-A nucleosomes in a complex with CENP-C^{CD} are found using either the human α-satellite DNA sequence that corresponds to the most heavily occupied site at centromeres (*7*) or the completely synthetic "601" nucleosome positioning sequence (*8*) (Fig. 1).

The shape change that we measure within the nucleosome upon CENP-C^{CD} binding most likely occurs through rotation at the four-helix bundles between histone dimer pairs within the octameric core, with interhistone contacts being stabilized or destabilized depending on the preference for rotational state. We tested this prediction using hydrogen/deuterium exchange-mass spectrometry (HXMS). Strong protection of CENP-A nucleosomes (Fig. 2A and figs. S3D and S4) is conferred by CENP-C^{CD} binding on peptides spanning helices that are predicted (*3*) to contact it (i.e., the α3 helix and C-terminal residues of CENP-A, the α2 helices of both H4 and H2A, and regions of H2A encompassing its acidic patch residues). In addition to the surface changes induced by CENP-C^{CD}, there are internal changes to the nucleosome that we measure by HX (Fig. 2, A and B, and movie S1) that are consistent with the change in nucleosome shape that we observed by FRET (Fig. 1). The separation of H2A/H2B dimers in CENP-A nucleosomes lacking CENP-C^{CD} (Fig. 1) is predicted to weaken an internal, intermolecular β sheet that serves as the physical connection between the H2A subunit on one face of the nucleosome and the H4 subunit on the opposite face. When CENP-C^{CD} binds to the CENP-A nucleosome, peptides spanning the corresponding β-sheet residues of both H2A and H4 exhibit extra protection from HX by 1 to 2 deuterons, where the same level of HX takes 5 to 10 times

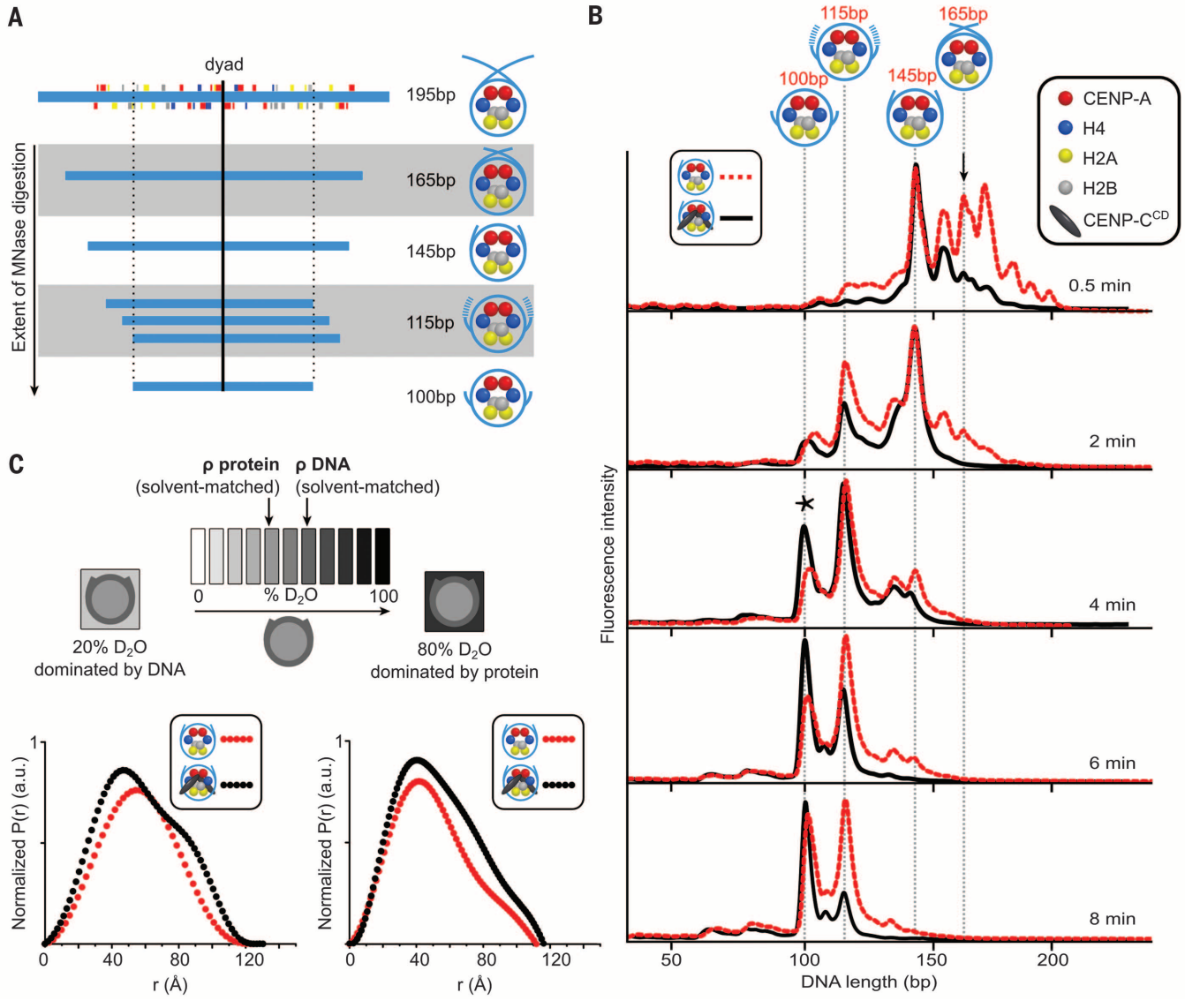

Fig. 3. Alterations in the nucleosome terminal DNA upon CENP-C^{CD} binding. (**A**) Major micrococcal nuclease (MNase)–digested DNA fragments observed for CENP-A nucleosomes assembled on its native centromere sequence. (**B**) MNase digestion profiles of CENP-A nucleosomes in the absence (red) and presence (black) of CENP-C^{CD}. The black arrow (0.5 min) points to the 165-bp peak (DNA crossed at the dyad). The asterisk (4 min) denotes the final 100-bp peak. (**C**) Scheme of SANS contrast variation experiment together with paired distance distribution curves for CENP-A nucleosomes alone (red) and bound by CENP-C^{CD} (black) in the indicated SANS contrast variation conditions.

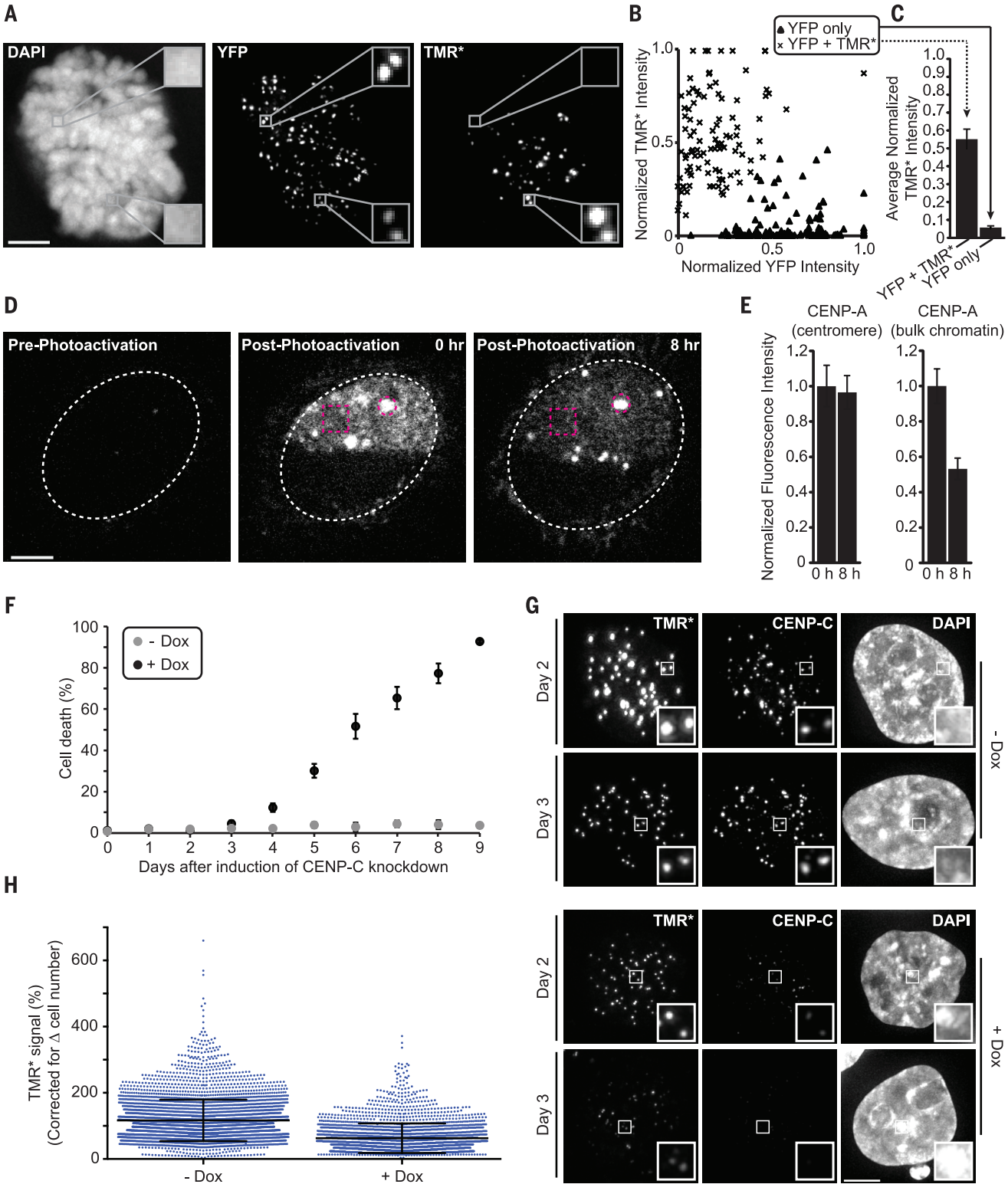

Fig. 4. Depletion of CENP-C reduces the high stability of CENP-A at centromeres. (**A** to **C**) Cells expressing SNAP-tagged CENP-A were pulse-labeled with TMR*, then fused with cells expressing YFP-tagged CENP-A. Representative images (A) show a cell in the second mitosis after fusion; insets show 3x magnification. X-means clustering was used to classify YFP only (triangles) or YFP and TMR* ("x" marks) centromeres (B), and mean (± SEM) TMR* intensity was calculated for each group (C). (**D** and **E**) Cells expressing high levels of CENP-A-PAGFP were photoactivated in bulk (box) and centromeric (circle) chromatin. Representative images (D) show a subset of centromeres in a single *z* section. Fluorescence intensity was quantified at 0 and 8 hours after photoactivation [(E), mean ± SEM]. (**F**) CENP-C knockdown begins causing cell death 4 days post-induction (mean ± SD). (**G** and **H**) Cells with (+ Dox) and without (– Dox) CENP-C depletion were pulse-labeled with TMR* (day 2), and the relative CENP-A-SNAP signals were analyzed (day 3). Quantification shows CENP-A-SNAP signal retained at day 3 (>2500 centromeres plotted with mean ± SD). Scale bars, 5 μm.

as long to occur than in CENP-A nucleosomes lacking CENP-C^{CD} (Fig. 2 and figs. S5 and S6).

Because CENP-C might also affect the extent that DNA wraps the nucleosomes, we reconstituted CENP-A nucleosomes using a 195–base pair (bp) DNA sequence from α-satellite DNA (*9*) that contains a contiguous sequence spanning the major binding site it occupies on human centromeres (*7*) (Fig. 3A). We first overdigested CENP-A nucleosomes and found very strong protection of 100 bp (fig. S9). Using a subsequent restriction digest of the 100-bp digestion product, we found that they were uniquely positioned, with their dyad precisely where the same-sized fragment previously mapped with native centromeric particles (*7*) (fig. S9). CENP-A–containing nucleosomes have many discrete intermediate digestion products before the strongly protected 100-bp fragment is generated (Fig. 3, A and B, and fig. S10). When CENP-C^{CD} is bound, digestion products larger than a nucleosome core particle [e.g., >145 bp, where DNA strands could cross at ~165 bp for conventional nucleosomes (*10*)] are missing at early time points (Fig. 3B). This suggests that when CENP-C^{CD} binds to the nucleosome, the DNA above the dyad rarely crosses, as it would normally cross for conventional nucleosomes. Second, digestion to the 100-bp final fragment proceeds more quickly (Fig. 3B). Thus, transient unwrapping of two helical turns (i.e., ~20 bp) from each terminus of the nucleosome is enhanced when CENP-C^{CD} is bound.

To determine whether CENP-C^{CD} binding leads to a steady-state structural change of nucleosomal DNA, we used small-angle neutron scattering (SANS) with contrast variation. When CENP-C^{CD} binds to CENP-A nucleosome core particles, the distance distribution profiles reflecting the shape in solution substantially redistribute for both the protein- and DNA-dominated measurements (Fig. 3C, fig. S11, and table S3). The increase in larger interatomic vectors for the protein component is expected to accompany an additional component (CENP-C^{CD}). The pronounced redistribution of vectors to both smaller and larger distances in DNA-dominated scattering when CENP-C^{CD} is bound is attributed to compaction of the nucleosome core (smaller vectors) and opening of the nucleosome terminal DNA when CENP-C^{CD} is bound (larger vectors).

We took two complementary approaches in cells to determine whether CENP-A is stably retained at the centromere upon which it is initially deposited (see the legend for fig. S12 that describes the motivation for these experiments). First, we used cell cycle–synchronized fluorescence pulse labeling of CENP-A in "donor" cells and subsequent cell fusion with an "acceptor" cell line. The donor cells express SNAP-tagged CENP-A that has been pulse labeled with tetramethylrhodamine-Star (TMR*) to irreversibly label CENP-A (*11*) before cell fusion. The acceptor cells express yellow fluorescent protein (YFP)–tagged CENP-A that is loaded at all centromeres, continuing even after fusion. At time points through the subsequent cell cycle (fig. S12) until the second mitosis (Fig. 4A), we observed no detectable exchange of the TMR*-labeled donor CENP-A to the acceptor centromeres in a shared nucleoplasm. Quantitation of the fluorescence at each centromere in these heterokaryons yields a bimodal distribution. The donor centromere group with high TMR* and low YFP (Fig. 4B, "x" symbols) has an average TMR* signal of 0.538 ± 0.005 (normalized arbitrary units where the maximal measured TMR* signal in each heterokaryon equals 1) (Fig. 4C), whereas the acceptor centromere group with high YFP and low TMR* (Fig. 4B, triangle symbols) has an average TMR* signal of 0.055 ± 0.005 (Fig. 4C). These data indicate that once assembled at a centromere, an individual CENP-A molecule is stably maintained at that particular centromere.

As a complementary approach to test CENP-A stability at individual centromeres, we used a photoactivatable version of CENP-A (CENP-A-PAGFP). We induced expression of CENP-A to the extent that it is present at locations throughout the nucleus, but with clear enrichment at centromeres, and then activated a defined region of each cell nucleus (Fig. 4D, 0 hours postphotoactivation). CENP-A-PAGFP signal is quantitatively retained at the activated centromeres and does not accumulate at unactivated centromeres (Fig. 4, D and E), indicating that there is negligible exchange between centromeres, consistent with our cell fusion results. In contrast, CENP-A-PAGFP signal in bulk chromatin decays, with about half of the protein removed by 8 hours after photoactivation.

To investigate whether CENP-C stabilizes CENP-A at centromeres, we combined SNAP labeling of CENP-A with CENP-C depletion (Fig. 4), for which we generated a cell line with a chromosomally integrated, doxycycline-inducible CENP-C short hairpin RNA cassette. In our SNAP system, CENP-C depletion leads to a dramatic decrease in the retention over 24 hours of the existing pool of CENP-A at centromeres (Fig. 4, G and H). Without CENP-C depletion, the average retention of CENP-A is slightly >100% (112% ± 63% SD), an increase that is explained by having a small pool of prenucleosomal CENP-A in the cell population that is labeled by the TMR* pulse and subsequently incorporated into centromeres. Nascent CENP-A deposition is also decreased when CENP-C is depleted (fig. S16C)—consistent with its proposed role in the CENP-A assembly reaction (*12*, *13*)—but this would only affect incorporation of the small prenucleosomal pool in the CENP-A retention measurements (Fig. 4, G and H). Thus, our findings implicate CENP-C in stabilizing CENP-A nucleosomes at centromeres. We cannot rule out the possibility that removal of CENP-C in turn removes another centromere component that stabilizes CENP-A nucleosomes, but we favor the idea that CENP-C is the key molecule for stabilizing CENP-A nucleosomes based on its direct binding to it.

CENP-A nucleosomes are highly stable at the centromeres upon which they are initially assembled. This stability is possible through collaboration with CENP-C. Along with the intranucleosomal rigidity of CENP-A and histone H4, where the key interfacial amino acids are important for accumulation at centromeres (*6*, *14*, *15*), the physical changes imposed by CENP-C combine to make CENP-A nucleosomes at centromeres very long-lived (fig. S21). Our data support a model of a steady-state octameric histone core where H2A/H2B dimers can exchange from either terminus of the CENP-A nucleosome. At the center, there is an essentially immobile $(CENP\text{-}A/H4)_2$ heterotetramer (*16*) (Fig. 4 and figs. S12 to S14). Thus, the physical properties related to CENP-A nucleosome stability at centromeres are tied to the intrinsic properties of the $(CENP\text{-}A/H4)_2$ heterotetramer (*6*, *14*, *15*) and the extrinsic properties imposed by CENP-C (Figs. 1 to 3 and fig. S21).

REFERENCES AND NOTES

1. B. E. Black, D. W. Cleveland, *Cell* **144**, 471–479 (2011).
2. C. W. Carroll, K. J. Milks, A. F. Straight, *J. Cell Biol.* **189**, 1143–1155 (2010).
3. H. Kato *et al.*, *Science* **340**, 1110–1113 (2013).
4. H. Tachiwana *et al.*, *Nature* **476**, 232–235 (2011).
5. K. Luger, A. W. Mäder, R. K. Richmond, D. F. Sargent, T. J. Richmond, *Nature* **389**, 251–260 (1997).
6. N. Sekulic, E. A. Bassett, D. J. Rogers, B. E. Black, *Nature* **467**, 347–351 (2010).
7. D. Hasson *et al.*, *Nat. Struct. Mol. Biol.* **20**, 687–695 (2013).
8. P. T. Lowary, J. Widom, *J. Mol. Biol.* **276**, 19–42 (1998).
9. J. M. Harp *et al.*, *Acta Crystallogr. D Biol. Crystallogr.* **52**, 283–288 (1996).
10. R. D. Kornberg, *Annu. Rev. Biochem.* **46**, 931–954 (1977).
11. L. E. T. Jansen, B. E. Black, D. R. Foltz, D. W. Cleveland, *J. Cell Biol.* **176**, 795–805 (2007).
12. S. Erhardt *et al.*, *J. Cell Biol.* **183**, 805–818 (2008).
13. B. Moree, C. B. Meyer, C. J. Fuller, A. F. Straight, *J. Cell Biol.* **194**, 855–871 (2011).
14. E. A. Bassett *et al.*, *Dev. Cell* **22**, 749–762 (2012).
15. B. E. Black *et al.*, *Nature* **430**, 578–582 (2004).
16. D. L. Bodor, L. P. Valente, J. F. Mata, B. E. Black, L. E. T. Jansen, *Mol. Biol. Cell* **24**, 923–932 (2013).

ACKNOWLEDGMENTS

We thank our University of Pennsylvania colleagues (J. Bell, C. Bialas, J. DeNizio, Y. Goldman, W. Hu, L. Lippert, L. Mayne, T. Panchenko, B. Türegün, and Z. Zhao) and S. Krueger and K. Sarachan [National Institute of Standards and Technology (NIST)] for assistance and advice with experiments; A. Straight (Stanford) for reagents and advice; and D. Cleveland (University of California, San Diego), J. Lippincott-Schwartz (NIH), K. Luger (Colorado State University), and E. Makeyev (Nanyang Technical University) for reagents. This work was supported by NIH grant GM082989 (B.E.B.), European Research Council grant ERC-2013-CoG-615638 (L.E.T.J.), predoctoral fellowships from the American Heart Association (E.M.S.) and NIH (CA186430, L.Y.G.), and a postdoctoral fellowship from the American Cancer Society (N.S.). We acknowledge support from NIH grants GM008275 (UPenn Structural Biology Training Grant, L.Y.G. and E.M.S), GM008216 (UPenn Genetics Training Grant, S.J.F.), and GM007229 (UPenn Cell and Molecular Biology Training Grant, G.A.L.). This work used facilities supported in part by NSF (agreement DMR-0944772). We acknowledge the support of NIST in providing the neutron research facilities used in this work.

SUPPLEMENTARY MATERIALS

www.sciencemag.org/content/348/6235/699/suppl/DC1
Materials and Methods
Figs. S1 to S21
Tables S1 to S3
Movie S1
References (*17*–*56*)

28 July 2014; accepted 7 April 2015
10.1126/science.1259308

Science

CENP-C reshapes and stabilizes CENP-A nucleosomes at the centromere

Samantha J. Falk, Lucie Y. Guo, Nikolina Sekulic, Evan M. Smoak, Tomoyasu Mani, Glennis A. Logsdon, Kushol Gupta, Lars E. T. Jansen, Gregory D. Van Duyne, Sergei A. Vinogradov, Michael A. Lampson and Ben E. Black

Science **348** (6235), 699-703.
DOI: 10.1126/science.1259308

Building stable centromeres

Each of our chromosomes has a single centromere, seen as a constriction during cell division, which is required for accurate chromosome segregation to daughter cells. Falk *et al.* show that the special histone protein known as CENP-A, which forms part of the nucleosomes at centromeres, makes the chromatin at these constrictions very stable and long-lived. This stability is conferred by a protein-binding partner, CENP-C, recruited to the centromere by the CENP-A histone. Binding of CENP-C to CENP-A–containing nucleosomes alters the behavior of the macromolecular centromere complex to help it maintain its identity

Science, this issue p. 699

Supplementary Materials for

CENP-C reshapes and stabilizes CENP-A nucleosomes at the centromere

Samantha J. Falk, Lucie Y. Guo, Nikolina Sekulic, Evan M. Smoak, Tomoyasu Mani, Glennis A. Logsdon, Kushol Gupta, Lars E. T. Jansen, Gregory D. Van Duyne, Sergei A. Vinogradov, Michael A. Lampson, Ben E. Black*

*Corresponding author. E-mail: blackbe@mail.med.upenn.edu

Published 8 May 2015, *Science* **348**, 699 (2015)
DOI: 10.1126/science.1259308

This PDF file includes:

Other Supplementary Material for this manuscript includes the following:
(available at www.sciencemag.org/cgi/content/full/348/6235/699/DC1)

Materials and Methods

FRET experiments. Recombinant human H2B was mutated using QuikChange (Stratagene) to contain a single cysteine (K120C or S123C) and then purified as described for the wildtype H2B (*6*). Lyophilized protein was dissolved in unfolding buffer (6 M Gnd-HCl, 10 mM Tris-HCl pH 7.5 at 20ºC, 0.4 mM TCEP) for 1 hr at RT and a 30-molar excess of either maleimido coumarin 343 (C343) or maleimido rhodamine B (RhB) dissolved in DMF was added dropwise to the protein. The reaction proceeded overnight shielded from light and was quenched with 10 mM DTT and run over a PD-10 column (GE Healthcare) to separate out free dye. Labeled H2B was then mixed with equimolar amounts of H2A for dimer reconstitution and purification using previously established methods (*6*, *17*). Labeling efficiencies, E, ranged from 45-90% and were calculated by spectroscopy using the Beer-Lambert law using the following equation (*18*):

$$E = [(A_{280} - (CF\ A_{max})/\varepsilon_{protein}l]/(A_{max}/\varepsilon_{fluorophore}l) \quad (1)$$

where A_{280} is the absorbance of protein at 280 nm, A_{max} is the absorbance of fluorophore at its maximum wavelength, $\varepsilon_{protein}$ and $\varepsilon_{fluorophore}$ are the molar extinction coefficients for protein and fluorophore, respectively, l is the pathlength, and CF is the correction factor for contribution to the protein A_{280} from the fluorophore. Labeling efficiency was further confirmed by SDS-PAGE (coomassie blue staining) and mass spectrometry (figs. S1 and S2). α-satellite DNA derived from a sequence described by Harp, *et al.* (*9*) or the 601 DNA sequence described by Lowary and Widom (*8*) were used in nucleosome assembly reactions. Briefly, a 145 bp region derived from a human α-satellite sequence with 25 bp of flanking DNA on each side was cloned into the pUC19 plasmid using EcoRI and XbaI restriction sites. The α-satellite DNA monomer was then amplified from the plasmid by PCR using primers specific to the flanking DNA regions. The complete α-satellite sequence is: 5'-CGTATCGCCTCCCTCGCGCCATCAG ATCAATATCCACCTGCAGATTCTACCAAAAGTGTATTTGGAAACTGCTCCATCAAAA GGCATGTTCAGCTCTGTGAGTGAAACTCCATCATCACAAAGAATATTCTGAGAATGC TTCCGTTTGCCTTTTATATGAACTTCCTGATCTGAGCGGGCTGGCAAGGCGCATAG-3', with the 145 bp α-satellite region underlined. Typically, DNA from multiple 96-well PCR reactions were pooled, ethanol precipitated, resuspended in TE buffer and purified by anion-exchange chromatography. Widom 601 DNA was purified as described (*7*). Nucleosomes were assembled on either DNA sequence and uniquely positioned using the gradual salt dialysis method followed by thermal shifting for 2 hr at 55ºC (*17*). Assembly was assessed by native PAGE (ethidium bromide and coomassie blue staining) and by SDS-PAGE (coomassie blue staining). As mentioned above, the fluorophores for FRET measurements were C343, serving as

an energy donor (D), and RhB, serving as an acceptor (A). C343 and RhB were selected because their calculated R_0 (Förster radius; distance at which energy transfer efficiency is 50%) is 58 Å, which is within the range of predicted dimer distances where energy transfer would be most sensitive to changes in FRET efficiency. For synthesis of fluorophores, all solvents and reagents were obtained from standard commercial sources and used as received. Selecto silica gel (Fisher Scientific, particle size 32-63 μm) was used for column chromatography. ^{1}H NMR spectra were recorded on a Varian Unity 400 MHz spectrometer. Mass spectra were obtained on a MALDI-TOF MS Microflex LRF instrument (Bruker Daltonics), using α-cyano-4-hydroxycinnamic acid as a matrix. The compound maleimido C343 was synthesized by a CDMT-assisted peptide coupling of C343 and 1-(2-Aminoethyl)pyrrol-2,5-dione. 1-(2-Aminoethyl)pyrrol-2,5-dione was synthesized as described (*19*). C343 was dissolved in DMF at 0°C, 2-chloro-4,6-dimethoxy-1,3,5-triazine and N-methylmorpholine (NMM) were added, and the mixture was stirred for 1 hr. 1-(2-Aminoethyl)pyrrol-2,5-dione and NMM were dissolved separately in DMF and added dropwise to the C343 mixture. The reaction was stirred at 0°C for 2 hr and then warmed to room temperature and stirred for 12 hr. The solvent was removed under vacuum and the residue was purified by column chromatography (silica gel, DCM). The fraction containing maleimido C343 was collected, the solvent was evaporated, and the product was dried under vacuum. ^{1}H NMR ($CDCl_3$, δ): 8.94 (s, 1H), 8.57 (s, 1H), 6.99 (d, 2H, ^3J = 3.5 Hz), 6.70 (s, 2H), 3.80 (t, 1H, ^3J = 5.8 Hz), 3.65 (m, 2H), 3.34 (m, 4H), 2.88 (t, 2H, ^3J = 6.3 Hz), 2.77 (t, 2H, ^3J = 6.1 Hz), 1.97 (m, 4H). For MALDI-TOF, the m/z (mass-to-charge ratio) calculated for $C_{22}H_{21}N_3O_5$ was 407.15; the following species were found; 407.102 [M]+ and 429.767 [M+Na]+. Maleimido RhB was synthesized by a HBTU-assisted peptide coupling of RhB piperazine amide (*20*) and N-maleimidoglycine (*21*). ^{1}H NMR ($CDCl_3$, δ): 7.78-7.72 (m, 3H), 7.53-7.51 (m, 1H), 7.29 (m, 2H), 7.10-7.05 (br s, 2H), 6.72 (s, 2H), 6.70 (s, 2H), 4.38 (s, 2H), 3.66-3.55 (m, 8H), 3.49-3.41 (m, 8H) 1.33 (t, 12H, ^3J = 7 Hz). For MALDI-TOF, the m/z calculated for $C_{38}H_{42}N_5O_5^+$ was 648.32; the following species were found; 648.358. Steady-state emission measurements were performed on a FS900 spectrofluorometer (Edinburgh Instruments), equipped with a photon-counting R2658P PMT (Hamamatsu). Samples were excited at 450 nm, the wavelength at which the absorbance of an equimolar mixture of C343 and RhB is dominated by C343 (>99%), and measurements were performed using dilute solutions (OD_{max}< 0.1) in a Spectrosil quartz cuvette (1 cm optical path length, Starna Cells). As a result, only negligible RhB emission is observed under these conditions in the absence of FRET. Emission spectra were corrected by the detector quantum yield and normalized by the incident light intensity at the excitation wavelength. The final emission spectra used in quantum yield calculations (see below) are expressed in counts (photons) per second (CPS). Absorbance measurements were performed using a LAMBDA 35 UV/Vis spectrophotometer (PerkinElmer). FRET efficiency was calculated based on donor

quenching in the presence of an acceptor fluorophore (*22–24*). The quantum yield of fluorescence was calculated using the following equation (*25*):

$$\Phi_S = \Phi_R[(A_R(\lambda_R)/A_S(\lambda_S)][n_S^2/n_R^2][D_S/D_R] \quad (2)$$

where Φ is quantum yield, $A(\lambda)$ is the absorbance value at the designated excitation wavelength, n is the refractive index of the solution (n_S = 1.333 and n_R = 1.361), and D is the integrated emission spectrum. The subscripts S and R refer to the sample and reference solutions, respectively. Rhodamine 6G in 100% ethanol was used as a reference actinometer (Φ_R= 0.95) (*26*).

Because of the nature of nucleosome reconstitutions, nucleosomes reconstituted with both C343- and RhB-labeled dimers (i.e. our FRET samples) contain some percentage of C343-only nucleosomes. Both C343- and RhB-labeled dimers exhibited ~90% labeling efficiency, meaning that ~10% of the dimers used in a reconstitution reaction are unlabeled. This leads to a mixture of nucleosomes characterized by the following equation:

$$UU + DU + DD + DA + AA + AU = 1 \quad (3)$$

where UU represents the subset of nucleosomes that contain two unlabeled dimers, DU represents the subset of nucleosomes that contain one C343-labeled dimer and one unlabeled dimer, DD represents the subset of nucleosomes with two C343-labeled dimers, DA represents the subset of nucleosomes with one C343-labeled dimer and one RhB-labeled dimer, AA represents the subset of nucleosomes with two RhB-labeled dimers, and AU represents the subset of nucleosomes with one RhB-labeled dimer and one unlabeled dimer. Because we are using donor quenching to calculate FRET efficiency, we only consider C343-containing species, so equation 3 is simplified to the following equation:

$$a + b = 1 \quad (4)$$

where a represents the normalized population of DU and DD nucleosomes and b represents the normalized population of DA nucleosomes in the FRET sample. Both a and b can be calculated using the known labeling efficiencies of both donor-labeled and acceptor-labeled dimers determined from spectroscopy and mass spectrometry analysis.

In order to account for the subset of DU and DD nucleosomes present in our FRET samples when measuring donor quenching, a separate control sample of C343-only nucleosomes are reconstituted and measured alongside every experimental sample. The following equation is then

used to calculate the quantum yield of C343 in nucleosomes containing both C343 and RhB dimers:

$\Phi_{DA} = [\Phi_T - a(\Phi_{DD})]/b$ (5)

where Φ_{DA} is the quantum yield of C343-RhB nucleosomes (DA), Φ_T is the total quantum yield of all C343-containing nucleosomes (DU + DD + DA), Φ_{DD} is the quantum yield of C343-only nucleosomes (DU + DD), and a and b represent the fraction of C343-only nucleosomes and C343-Rhb nucleosomes in a sample, respectively, determined as described above. Φ_T and Φ_{DD} are calculated from the FRET sample and the C343-only sample, respectively, using equation 2 above.

FRET efficiency, Φ_{FRET}, is then determined based on the following equation (*18*):

$\Phi_{FRET} = 1-(\Phi_{DA}/\Phi_{DD})$ (6)

The distance, r, between the two fluorophores is then calculated using the following equation (*18*):

$r = R_0[(1/\Phi_{FRET})-1]^{1/6}$ (7)

where R_0 is the Förster radius. For the C343/RhB pair, the R_0 was calculated to be 58 Å, using the following equation (*18*):

$R_0 = 9790(J\kappa^2\Phi_{DD}n^{-4})^{1/6}$ Å (8)

where J is the spectral overlap integral for C343/RhB pair, Φ_{DD} is the quantum yield of C343, n is the refractive index of the solvent (n=1.333), and $\kappa^2=2/3$ is the orientation factor for freely rotating fluorophores (*18*). Our assumption of orientational averaging as in the case of freely rotating transition dipole moments was confirmed by our anisotropy measurements (see below). The measured anisotropy for the fluorophore pair was found to be less than 0.2 (fig. S1 and Table S1), confirming that usage of formula (7) was appropriate for estimation of interchromophoric distances. Steady-state fluorescence anisotropy measurements were performed on a QuantaMaster spectrophotometer (PTI). Samples were diluted to 0.5-1.0 μM in 150 mM NaCl, 20 mM Tris-HCl pH 7.5 at 4°C, 1 mM EDTA, 1 mM DTT and excited at 450 nm for C343 and 567 nm for RhB. Anisotropy, r, was calculated in FeliX32 software using the following equation (*18*):

$r = (I_{VV} – G\ I_{VH})/(I_{VV} + 2G\ I_{VH})$ (9)

where I_{VV} is the parallel polarized fluorescence intensity, I_{VH} is the perpendicular polarized fluorescence intensity, and G is the correction factor for the setup. Lifetime measurements, τ, were performed using a FluoroLog fluorometer (Horiba Scientific). The excitation source was an LED (NanoLED), l_{max}=441 nm with an average repetition rate of 1 MHz. Samples were in 150 mM NaCl, 20 mM Tris-HCl pH 7.5 at 4°C, 1 mM EDTA, 1 mM DTT at 0.5-1.0 μM. Emission was measured at 491 nm using a bandpass filter (5 nm). Lifetimes were fitted exponentially using DAS6 software (Horiba Scientific).

HXMS. CENP-A mononucleosomes were reconstituted with the same 195 bp α-satellite DNA described above in the FRET studies and concentrated to 0.9 mg/ml with Centricon concentrators (Millipore, Billerica, MA). Recombinant human CENP-C^{CD} consisting of the central domain only (a.a. 426-537, the plasmid for recombinant human CENP-C^{CD} expression was a generous gift from A. Straight, Stanford, USA) was GST-tagged and purified over a GST column followed by PreScission protease cleavage (GE Healthcare) and ion-exchange chromatography and prepared in a buffer containing 20 mM Tris pH 7.5, 200 mM NaCl, 0.5 mM EDTA, 1 mM DTT. To form complexes with CENP-C^{CD}, 2.2 moles of recombinant CENP-C^{CD} were added per mole of CENP-A nucleosomes. To the nucleosome-only sample the buffer used for CENP-C^{CD} preparation was added so that the chemical composition of the buffers were identical in all cases. Deuterium on-exchange was carried out by adding 5 μL of each sample (containing approximately 4 μg of nucleosomes or complex) to 15 μL of deuterium on-exchange buffer (10 mM Tris, pD 7.5, 0.5 mM EDTA, in D_2O) so that the final D_2O content was 75%. Reactions were quenched at the indicated time points by withdrawing 20 μL of the reaction volume, mixing in 30 μL ice cold quench buffer (2.5 M GdHCl, 0.8% formic acid, 10% glycerol), and rapidly freezing in liquid nitrogen prior to proteolysis and LC-MS steps. HX samples were individually melted at 0°C then injected (50 μl) and pumped through an immobilized pepsin (Sigma) column at initial flow rate of 50 μl/min for 2 min followed by 150 μl/min for another 2 min. Pepsin was immobilized by coupling to Poros 20 AL support (Applied Biosystems) and packed into column housings of 2 mm x 2 cm (64 μL) (Upchurch). Protease-generated fragments were collected onto a C18 HPLC trap column (800 μm x 2 mm, Dionex) and eluted through an analytical C18 HPLC column (0.3 x 75 mm, Agilent) by a linear 12-55% buffer B gradient at 6 μl/min (Buffer A: 0.1% formic acid; Buffer B: 0.1% formic acid, 99.9% acetonitrile). The effluent was electrosprayed into the mass spectrometer (LTQ Orbitrap XL, Thermo Fisher Scientific). The SEQUEST (Bioworks) software program was used to identify the likely sequence of parent peptides using nondeuterated samples via tandem MS. MATLAB based MS data analysis tool, ExMS, was used for data processing (*27*).

MNase digestions. Nucleosomes were assembled using the same 195 bp α-satellite DNA sequence used in FRET studies using the same assembly approach described above. Nucleosomes were digested for various times with 2 U/μg of MNase (Roche) at room temperature (22°C). Reactions were terminated with the addition of guanidine thiocyanate and EGTA. The DNA was isolated using a MinElute PCR purification kit (Qiagen) and analyzed on an Agilent 2100 Bioanalyzer.

SANS. Nucleosome core particles were assembled on the α-satellite 145 bp sequence described above. The sequence was cloned in tandem copies separated by EcoRV sites in pUC57. The 145 bp fragments were released by EcoRV digestion and purified away from the backbone by anion exchange chromatography. Following nucleosome reconstitutions, performed as described above, the nucleosomes were purified by preparative electrophoresis (Prep Cell, BioRad) using a 5% native gel to separate free DNA and any other non-nucleosomal species (*17*). SANS experiments were performed at the National Institutes of Standards and Technology Center for Neutron Research NG-3. Samples were prepared by dialysis at 4ºC against matching buffers containing 20% or 80% D_2O for a minimum of 3 hr using a 6-8 kDa cutoff D-tube dialyzer (Novagen). Samples were centrifuged at 10,000 X g for 5 min at 4ºC and then loaded into Hellma quartz cylindrical cells (outside diameter of 22 mm) with 1 mm path lengths and maintained at 6ºC during the experiment. Sample concentrations were determined by Bradford analysis and optical absorbance at 260 nm. Scattered neutrons were detected with a 64 cm × 64 cm two-dimensional position-sensitive detector with 128 × 128 pixels at a resolution of 0.5 cm/pixel. Data reduction was performed using the NCNR Igor Pro macro package (*28*). Raw counts were normalized to a common monitor count and corrected for empty cell counts, ambient room background counts and non-uniform detector response. Data were placed on an absolute scale by normalizing the scattered intensity to the incident beam flux. Finally, the data were radially-averaged to produce scattered intensity, I(q), versus q curves. The scattered intensities from the samples were further corrected for buffer scattering and incoherent scattering from hydrogen in the samples. Data collection times varied from 0.5-2 hr, depending on the instrument configuration, sample concentration and buffer conditions. Sample-to-detector distances of 11 m (q-range 0.006-0.043 $Å^{-1}$, where $q = 4\pi\sin(\theta)/\lambda$, where λ is the neutron wavelength and 2θ is the scattering angle), 5 m (q-range 0.011–0.094 $Å^{-1}$), and 1.5 m (detector offset by 20.00 cm, q-range 0.03–0.4 $Å^{-1}$) at a wavelength of 6 Å and a wavelength spread of 0.15 were collected for each contrast point. We observed good agreement between Rg and I(0) values determined from either inverse Fourier analysis using GNOM or from Guinier analysis. The program MuLCH (*29*) was used to calculate theoretical contrast and to analyze contrast

variation data. Distance distribution curves were normalized for total molecular mass for the complex.

SNAP labeling experiments and cell fusions. CENP-A-SNAP HeLa cells for fusion experiments were labeled with TMR* (NEB) as described previously and subjected to a double thymidine block with a final thymidine concentration of 2 mM (*11*, *16*). YFP-CENP-A HeLa cells (*30*), CENP-A-SNAP Hela cells (*11*), and SNAP-tagged core histone (H3.1, H3.3, H4, and H2B)-expressing HeLa cells (*16*, *31*) are all established lines. After labeling with TMR*, CENP-A-SNAP HeLa cells were trypsinized, counted, and co-seeded onto poly-D-lysine (Sigma-Aldrich) treated coverslips along with an equivalent number of HeLa cells constitutively expressing YFP-CENP-A. Cells were arrested in growth medium (DMEM supplemented with 10% fetal bovine serum (FBS), 100 U/mL penicillin, and 100 μg/mL streptomycin) containing 2 mM thymidine for 17 hr. Cells were then washed 3x with PBS, fused with 50% PEG-1500 (Roche) for 30 s and subsequently washed in PBS and placed in media containing 24 μM deoxycytidine to release from thymidine block. After 9 hr, cells were blocked again with media containing thymidine for 17 hr. Cells were released from thymidine with DMEM media containing 24 μM deoxycytidine and nocodazole was added 7 hr post-release at a final concentration of 400 ng/mL. Coverslips were fixed and processed for immunofluorescence at the timepoints outlined in Fig. S12A. HeLa-based cell lines for inducible CENP-A-SNAP with and without shRNAs, and constitutive CENP-A-SNAP with inducible shRNAs directed against CENP-C were generated by recombinase-mediated cassette exchange (RMCE) using the HILO RMCE system (a generous gift from E.V. Makeyev, Nanyang Technological University, Singapore (*32*)). pEM784 was used to express nuclear-localized Cre recombinase. pEM791 was modified for inducible expression of CENP-A-SNAP-HA3, CENP-A-SNAP-HA3 plus 2 shRNAs against CENP-C (5'-tgctgttgactttctaccttgaaggagttttggccgctgactgactccttcaatagaaagtcaa-3' and 5'-tgctgacaagtttgttcttggactcagttttggccactgactgactgagtccaaacaaacttgt-3'), constitutive CENP-A-SNAP-HA3 driven by the EF1α promoter plus 2 shRNAs against CENP-C, and CENP-A-PAGFP respectively. CENP-C knockdown was induced in constitutive CENP-A-SNAP cell lines by treating for 48 hr with 2 μg/mL doxycycline prior to TMR* labeling for pulse-chase experiments to measure the retention of CENP-A protein at centromeres. Cells were fixed either immediately after labeling or again 24 hr later. Cell number was also determined at these time points, so that the total level of CENP-A turnover could be calculated, as described (*16*). For experiments to measure the amount of new CENP-A assembly with or without CENP-C knockdown, cells were treated with 50 ng/mL of doxycycline during a double thymidine block procedure that spanned 48 hr. Following release from the double thymidine block, CENP-A-SNAP was quenched with SNAP-Cell Block (NEB) then released for 6.5 hr to allow for new

synthesis of CENP-A-SNAP protein. The nascent pool of CENP-A-SNAP protein was then pulse-labeled with TMR*, and the cells were cultured for an additional 17.5 hr prior to fixation and processing for immunofluorescence. A separate sample was labeled with TMR* immediately after the quench step to confirm successful quenching of 'old' CENP-A. For immunofluorescence, cells were fixed in 4% formaldehyde for 10 min at room temperature followed by permeabilization using PBS + 0.5% Triton X-100. Samples were stained with DAPI before mounting with Vectashield medium (Vector laboratories). The following primary antibodies were used: mouse mAb anti-CENP-A (1:1000 Enzo), rabbit pAb anti-CENP-C (1:2000) (*33*), and mouse mAb anti-HA.II antibody (1:1000, Covance). AlexaFluor488- and AlexaFluor647-conjugated secondary antibodies were obtained from Invitrogen and were used at 1:1000. Images were captured at 23°C using software (LAF; Leica) by a charge-coupled device camera (ORCA AG; Hamamatsu Photonics) mounted on an inverted microscope (DMI6000B; Leica) with a 100x 1.4 NA objective. For each sample, images were collected at either 0.2 μm z-sections (Figs. 4A, S12-15,17) or 0.49 μm z-sections (Figs. 4D,G and S16) that were subsequently deconvolved using identical parameters. The z-stacks were projected as single two-dimensional images and assembled using PhotoShop (version 13.0; Adobe), ImageJ (1.48v) (*34*), and Illustrator (version 16.0; Adobe). To quantify fluorescence intensity in cell fusions, individual centromeres from non-deconvolved maximum projections were selected and the intensity of both TMR* and YFP signal were determined after subtracting the background fluorescence measured from adjacent regions of the cell using ImageJ. For each unique fusion, the levels of fluorescence for both channels were normalized to the highest measured value in that channel, leading to normalized values for YFP intensity and TMR* intensity for each centromere in the fused cell. Thus, each centromere is a data point that has an associated TMR* and YFP value assigned to it, which were then run through the machine learning x-means clustering algorithm of Weka (*35*, *36*), which partitions the data points into n clusters based on their closeness to an assigned mean value. This generated the two groups of data points (YFP only and YFP + TMR*) in the plot seen in Fig. 4B. To quantify fluorescence intensity in experiments with CENP-C knockdown, the Centromere Recognition and Quantification (CRaQ) macro (*37*) was run in ImageJ with standard settings using a reference channel and DAPI. Total CENP-A staining was used as the reference channel to define ROIs for quantification of TMR* intensity. CENP-A fluorescence intensity values at the final time point were normalized to reflect the total pool of labeled CENP-A by accounting for the increase in cell number in the dividing cell populations following TMR* pulse. 2800-4200 centromeres from >70 cells were analyzed for each time point.

PAGFP experiments. CENP-A-PAGFP cells were generated with the RMCE system (*32*), as described above, and expression was induced with 1 μg/mL doxycycline 2 days prior to photoactivation and continued for the duration of the experiment. Cells were cultured in growth medium at 37°C in a humidified atmosphere with 5% CO_2. For live imaging, cells were plated on 22 x 22 mm glass coverslips (#1.5; Thermo Fisher Scientific) coated with poly-D-lysine (Sigma-Aldrich). Coverslips were mounted in magnetic chambers (Chamlide CM-S22-1, LCI) using growth medium without phenol red (Invitrogen). Temperature was maintained at 37°C with 5% CO_2 using an environmental chamber (Incubator BL; PeCon GmbH). Evaporation of media was prevented by applying a thin layer of mineral oil over the media within the magnetic chamber. Prior to photoactivation, a single plane image of the unactivated nucleus was acquired to be used for background subtraction. Cells were subsequently photoactivated by defining an ROI surrounding ~half of the nucleus and then activated using a pointable 405 nm laser (CrystaLaser) set to 10% power and one repetition using iLAS^2 software run through MetaMorph, followed by acquisition of an image of a single z-plane. Cells were then followed by DIC for 8 hr, at which point a final single plane image was acquired. Images were acquired with a confocal microscope (DM4000; Leica) with a 100x 1.4 NA objective lens, an XY Piezo-Z stage (Applied Scientific Instrumentation), a spinning disk (Yokogawa Corporation of America), an electron multiplier charge-coupled device camera (ImageEM; Hamamatsu Photonics), and a laser merge module equipped with 488 nm and 593 nm lasers (LMM5; Spectral Applied Research) controlled by MetaMorph software (Molecular Devices). To quantify the retention of CENP-A-PAGFP in bulk chromatin, a 25 x 25 pixel region-of-interest (ROI) was drawn in ImageJ on a region of photoactivated bulk chromatin and the average fluorescence was recorded. Recorded fluorescence measurements were corrected for background by subtracting the fluorescence value of the pre-photoactivated ROI. This corrected average fluorescence of the ROI was then multiplied by the area of the ROI in order to calculate the average fluorescence of the area. These area fluorescence measurements of the bulk chromatin ROI for each cell were averaged to generate the final numbers for comparison. Upon overexpression, CENP-A initially assembles into nucleosomes at centromeres and at locations throughout the genome (*38, 39*). Functional centromeres do not spread throughout chromosomes under these conditions. We note that there is a small soluble pool of CENP-A in bulk chromatin that is mobile throughout the nucleus, but this does not significantly contribute to quantification and does not diffuse to the unactivated portion of the nucleus in earlier time points. To quantify the retention of CENP-A-PAGFP in centromeric chromatin, single planes were thresholded to create ROIs around all visibly photoactivated centromeres and the average fluorescence as well as the total centromeric area were both recorded. Fluorescence measurements were corrected for background by subtracting the fluorescence value of the pre-photoactivated ROIs. This corrected average

fluorescence of the ROI was then multiplied by the area of the ROIs in order to calculate the average fluorescence of the area. These area fluorescence measurements of the centromeric chromatin ROIs for each cell were averaged to generate the final numbers for comparison.

Cell lethality assay. Constitutive CENP-A-SNAP HeLa cells with doxycycline-inducible shRNAs directed against CENP-C were seeded in 6-well plates in triplicate at 8.4 x 10^4 cells per well and with daily introduction of 2 μg/mL dox. Cells were collected and stained with 0.4% Trypan Blue (CellGro) and counted on a hemocytometer to calculate the percentage of cell death based on trypan blue uptake.

Immunoblotting. Samples derived from whole cell lysates were separated by SDS-PAGE and transferred to a nitrocellulose membrane for immunoblotting. Blots were probed using the following antibodies: human ACA (2 μg/mL, Antibodies Incorporated), rabbit anti-CENP-C (1.7 μg/mL) and mouse mAb anti-α-tubulin (1:4000, Sigma-Aldrich). Antibodies were detected using a horseradish peroxidase-conjugated secondary antibody at 1:10,000 (human) and 1:2000 (rabbit or mouse) (Jackson ImmunoResearch Laboratories) and enhanced chemiluminescence (Thermo Scientific).

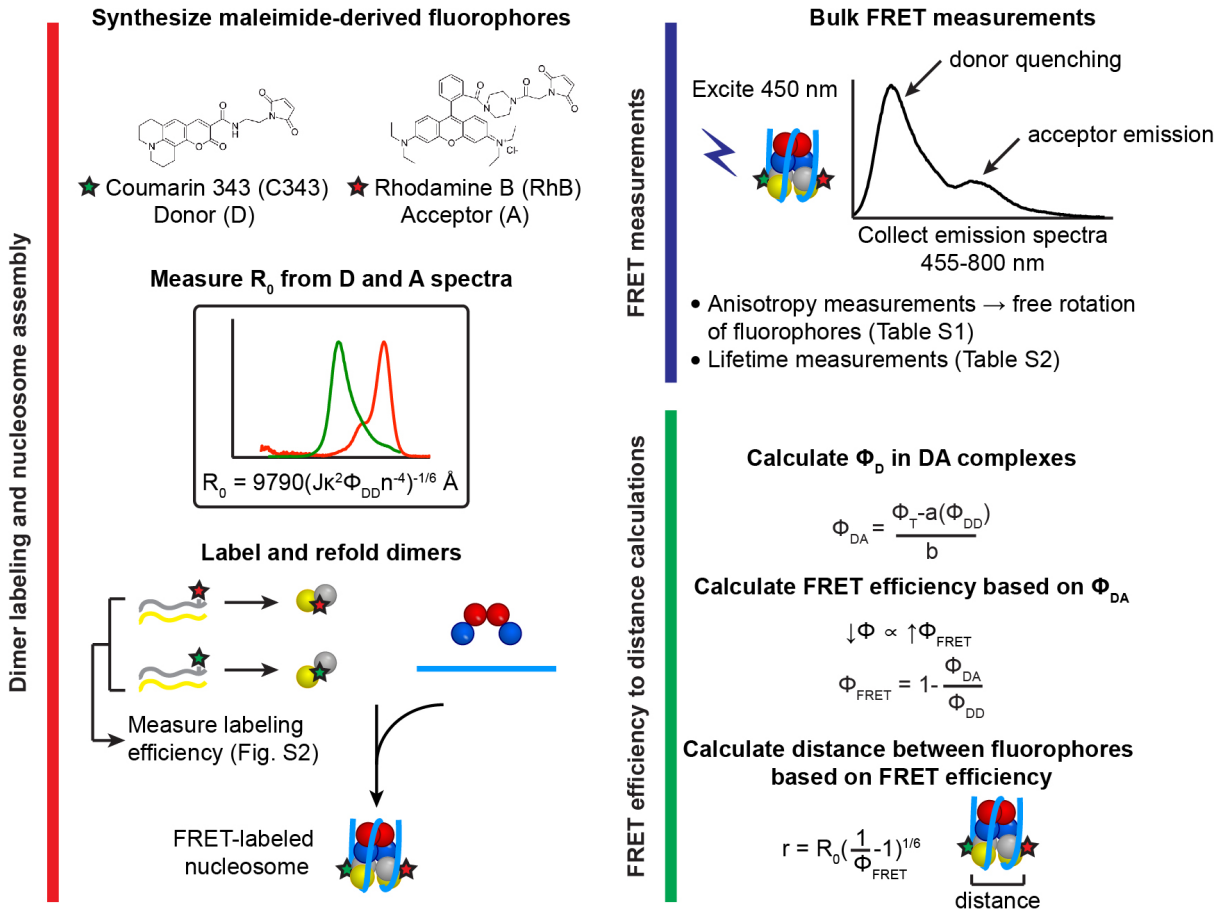

Fig. S1. Simplified schematic for assembly, measurement and calculation of FRET efficiency and distance between fluorophores.
For a detailed description of experimental methods and calculations, see Supplemental Methods. Definition of terms: D – donor, A – acceptor, R_0 – Förster distance, J – spectral overlap integral, κ^2 – dipole orientation factor, Φ_{DD} – quantum yield of D-only nucleosomes, n – refractive index, Φ_{DA} – quantum yield of DA nucleosomes, Φ_T – total quantum yield of all D-containing nucleosomes, a – correction factor for D-only nucleosomes, b – correction factor for DA nucleosomes, Φ_{FRET} – FRET efficiency, r – calculated distance between D and A.

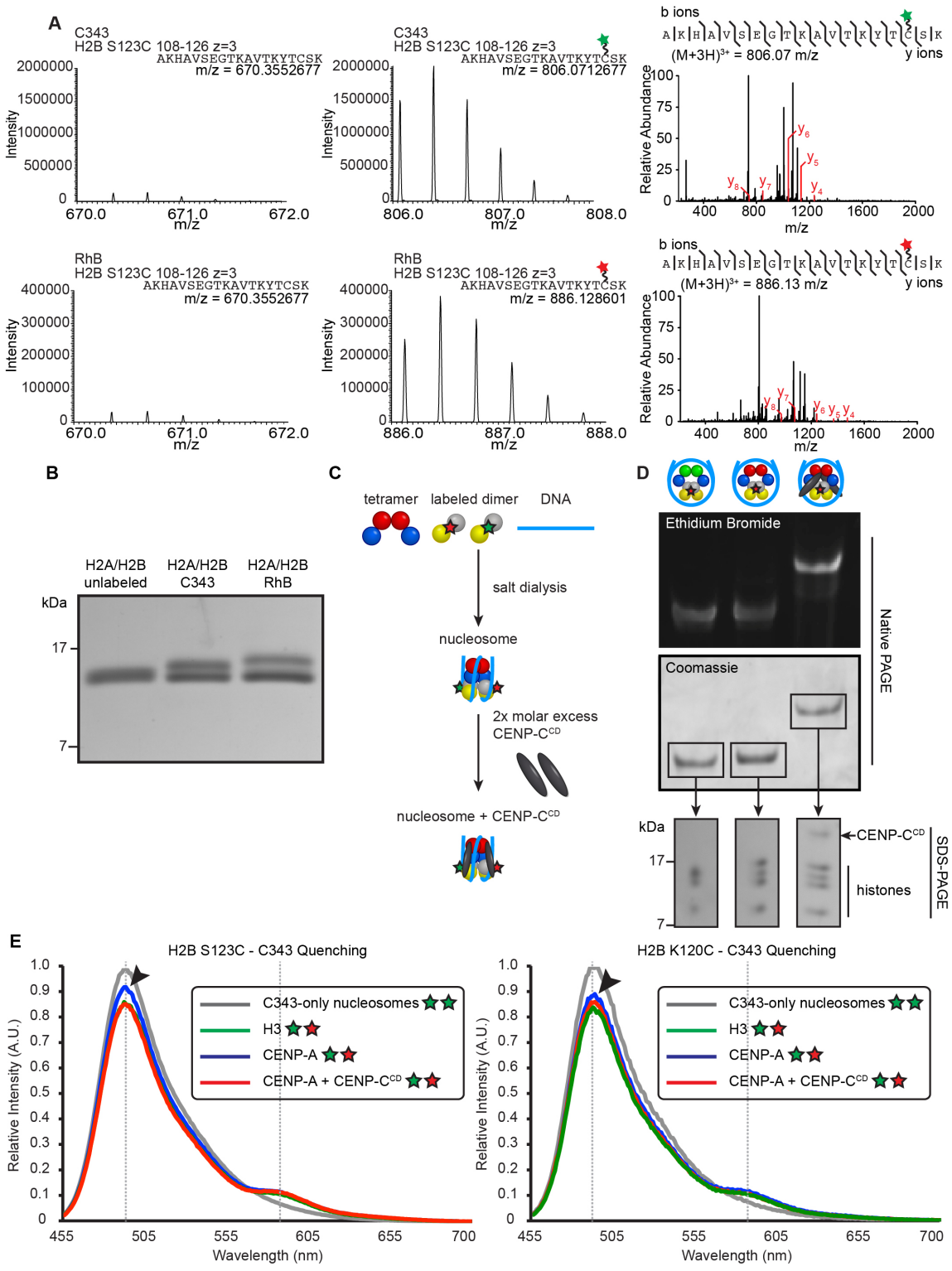

Fig. S2. **Assembly of fluorophore-labeled nucleosomes and FRET measurements.**
(**A**) Mass spectrometry of H2B labeled with C343 (top row) or RhB (bottom row). Left and middle panels, MS1 spectra for a representative peptide (108-126, z = +3) that contains the mutant cysteine labeled with fluorophore. Both unlabeled and labeled peptides were identified

from the same run, but the labeled peptide is present at a much higher signal, indicative of a high degree of labeling. Right, MS2 spectra of the labeled peptides from the middle panel. The lines between the amino acids indicate observed b ions (N-terminal) and y ions (C-terminal). The y ions highlighted in red contain the fluorophore of interest and were used to identify the MS1 spectra with high confidence. (**B**) Comparison of unlabeled, C343-, and RhB-labeled H2A/H2B dimers resolved by SDS-PAGE gel visualized with coomassie blue stain. Note that unlabeled H2A and H2B have the same mobility and appear as a single band. (**C**) Schematic for assembly of nucleosomes for FRET, followed by binding of CENP-C^{CD} to CENP-A-containing nucleosomes. (**D**) H3-containing nucleosomes, CENP-A containing nucleosomes, and CENP-A containing nucleosomes bound by CENP-C^{CD} were resolved by native PAGE and stained with ethidium bromide to visualize DNA content (top panel) and coomassie blue to visualize protein content (middle panel). Coomassie blue-stained bands were subsequently excised from the native gel and analyzed by SDS-PAGE to resolve the individual protein components (bottom panel). (**E**) Representative emission spectra demonstrating donor quenching in the presence of an acceptor for the indicated nucleosomes. Note that the C343 emission peak (λ_{max} = 491 nm, arrowhead) decreases in the presence of an acceptor and a RhB emission peak (λ_{max} = 567 nm) appears for all three nucleosome types whether H2B S123C (left) or H2B K120C (right) is used for fluorophore attachment, indicative of donor quenching due to FRET. For both labeling sites, CENP-A-containing nucleosomes have the least amount of reduction in C343 emission, indicating lower FRET efficiency compared to H3-containing nucleosomes and CENP-A-containing nucleosomes bound by CENP-C^{CD}. Each emission spectra is first normalized to the measured absorbance value of C343 in the specific nucleosome FRET sample, followed by normalization to the donor-only control spectra to show relative differences in donor quenching.

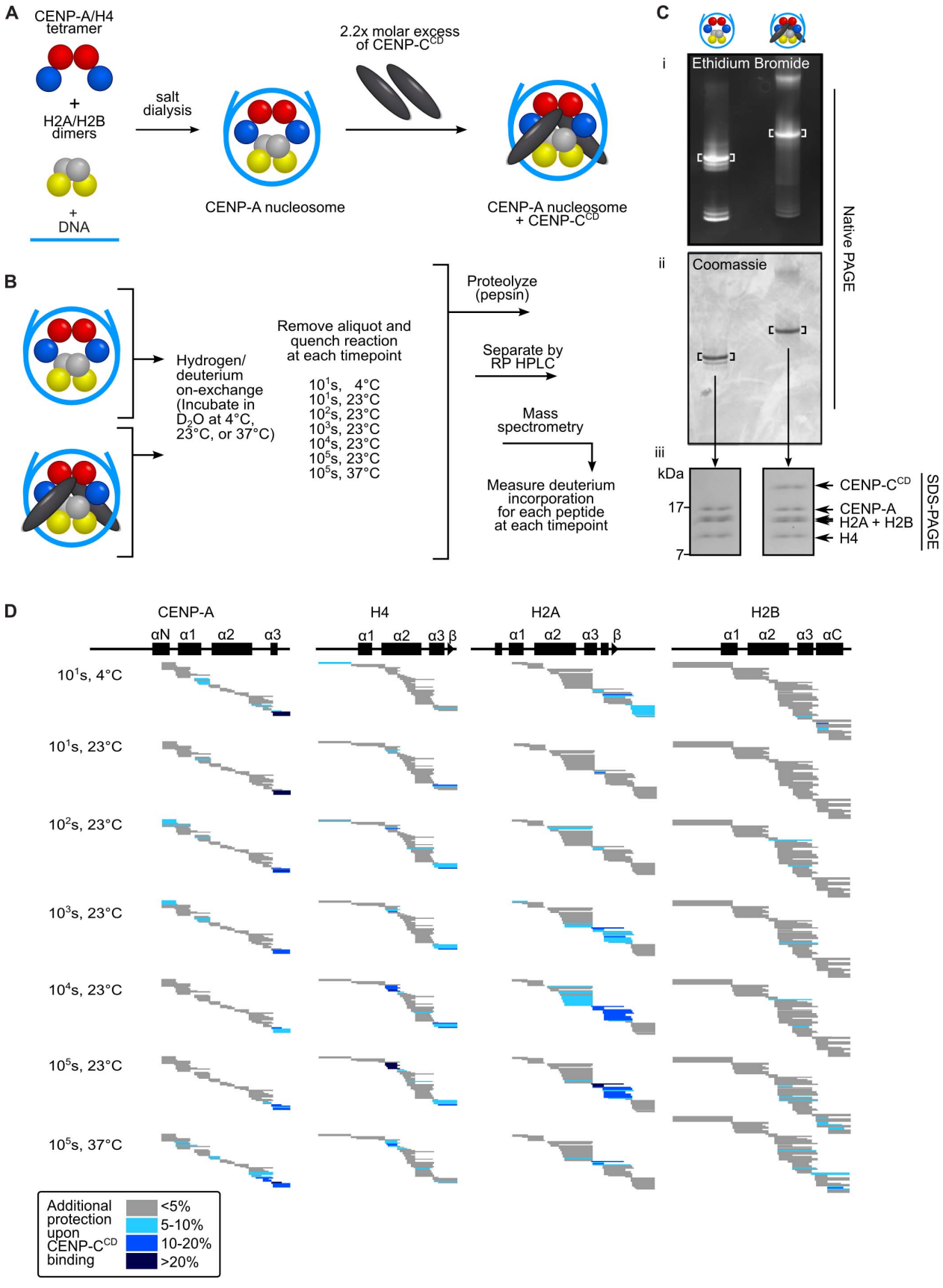
A
CENP-A/H4 tetramer
+
H2A/H2B dimers
+
DNA
salt dialysis
CENP-A nucleosome
2.2x molar excess of CENP-C^CD
CENP-A nucleosome + CENP-C^CD
B
Hydrogen/ deuterium on-exchange (Incubate in D2O at 4°C, 23°C, or 37°C)
Remove aliquot and quench reaction at each timepoint
10^1s, 4°C
10^1s, 23°C
10^2s, 23°C
10^3s, 23°C
10^4s, 23°C
10^5s, 23°C
10^5s, 37°C
Proteolyze (pepsin)
Separate by RP HPLC
Mass spectrometry
Measure deuterium incorporation for each peptide at each timepoint
C
i
Ethidium Bromide
ii
Coomassie
Native PAGE
iii
kDa
17
7
CENP-C^CD
CENP-A
H2A + H2B
H4
SDS-PAGE
D
CENP-A
αN α1 α2 α3
H4
α1 α2 α3 β
H2A
α1 α2 α3 β
H2B
α1 α2 α3 αC
10^1s, 4°C
10^1s, 23°C
10^2s, 23°C
10^3s, 23°C
10^4s, 23°C
10^5s, 23°C
10^5s, 37°C
Additional protection upon CENP-C^CD binding
<5%
5-10%
10-20%
>20%

Fig. S3. CENP-C^{CD} binding induces additional protection from HX at multiple regions within the CENP-A nucleosome.

(**A,B**) Experimental scheme for HXMS. HXMS is an approach that measures the exchange of amide protons along the polypeptide backbone of the histones with deuterons from heavy water (D_2O) in the exchange buffer (*40*). Amide protons engaged in hydrogen bonds inside α-helices and the interior of β-sheets are protected from HX, exchanging only upon transient unfolding of structure, and thus this technique detects stabilization/destabilization of these structures. (**C**) CENP-A nucleosome alone and in complex with CENP-C^{CD} as assessed by native gel stained with ethidium bromide (i) or coomassie blue (ii). Bands from native gel were excised and assessed by SDS-PAGE (iii). (**D**) Regions of CENP-A nucleosomes where CENP-C^{CD} binding leads to additional protection from HX. The level of protection added by the presence of CENP-C^{CD} is determined by subtracting the level of HX of the CENP-A nucleosome alone from that of CENP-A nucleosomes bound by CENP-C^{CD}. Each horizontal bar represents an individual peptide, placed beneath schematics of secondary structural elements of the CENP-A nucleosome. Peptides that exhibit additional protection from HX upon CENP-C^{CD} binding are colored in blue, with shading according to the legend. It is notable that prior to nucleosome assembly, CENP-A/H4 is protected from HX by HJURP (*14*), and after chromatin assembly CENP-A/H4, as well as the nucleosome subunit, H2A, is protected from HX by CENP-C^{CD} (this study). HJURP is thought to protect CENP-A/H4 during the long cell cycle window between when CENP-A is expressed in late S-phase (*41*) to when it is assembled at centromeres in the subsequent G1 (*11*). Our studies strongly suggest that CENP-C is important for stabilizing CENP-A nucleosomes at the centromere to maintain centromere identity.

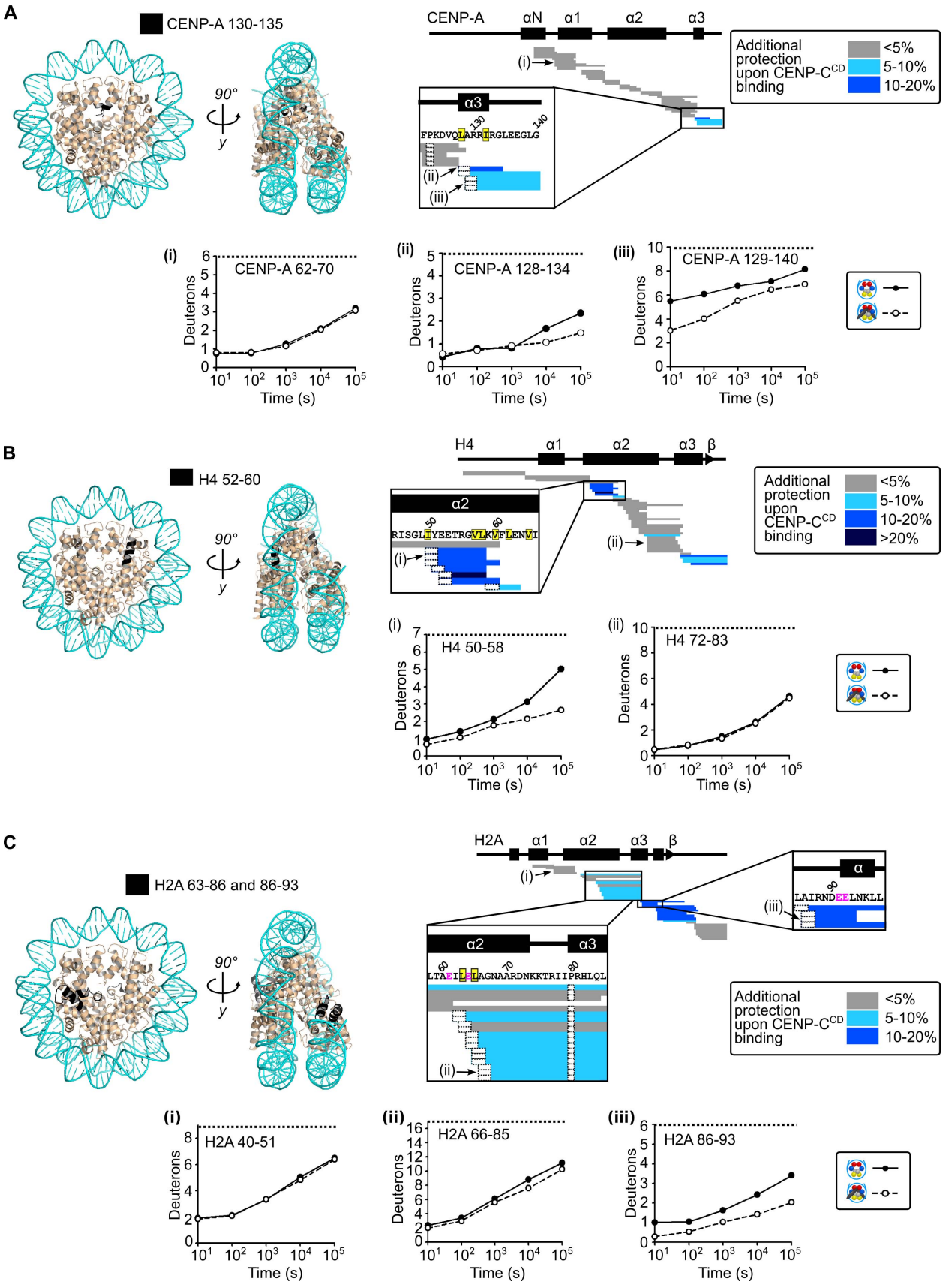
A
CENP-A 130-135
90°
y
CENP-A
αN
α1
α2
α3
(i)
α3
FPKDVQLARRIRGLEEGLG
130
140
(ii)
(iii)
Additional protection upon CENP-C^CD binding
<5%
5-10%
10-20%
(i)
CENP-A 62-70
(ii)
CENP-A 128-134
(iii)
CENP-A 129-140
Deuterons
Time (s)
B
H4 52-60
90°
y
H4
α1
α2
α3
β
α2
RISGLIYEETRGVLKVFLENVI
50
60
(i)
(ii)
Additional protection upon CENP-C^CD binding
<5%
5-10%
10-20%
>20%
(i)
H4 50-58
(ii)
H4 72-83
Deuterons
Time (s)
C
H2A 63-86 and 86-93
90°
y
H2A
α1
α2
α3
β
α
α2
α3
LTAEILHLAGNAARDNKKTRIIPRHLQL
60
70
80
LAIRNDEELNKLL
90
(i)
(ii)
(iii)
Additional protection upon CENP-C^CD binding
<5%
5-10%
10-20%
(i)
H2A 40-51
(ii)
H2A 66-85
(iii)
H2A 86-93
Deuterons
Time (s)

Fig. S4. Regions on the surface of the nucleosome that exhibit additional protection from HX upon CENP-C^{CD} binding.
(**A**) CENP-A 130-140, (**B**) H4 52-60, and (**C**) H2A 63-93, mapped in black onto the structure of the CENP-A nucleosome (PDB 3AN2). Horizontal blocks represent peptides from CENP-A-containing nucleosomes, placed beneath schematics showing locations of α-helices and β-sheets of each histone. Multiple charge states were detected for a subset of peptides, each represented by its own block. Representative peptides from these regions exhibiting protection or from flanking regions exhibiting no extra protection are plotted as the number of deuterons exchanged at each time point. The maximum number of deuterons for each peptide possible to measure by HXMS is shown by the dotted line. Residues highlighted in yellow are those that exhibited methyl chemical shift perturbation in the NMR model of $H3_{1\text{-}132}$LEEGLG nucleosome bound to CENP-C^{CD} (*3*). The glutamate residues in pink on H2A are acidic patch residues. Note that PDB 3AN2 does not contain CENP-A residues 136-140, thus only 130-135 are colored.

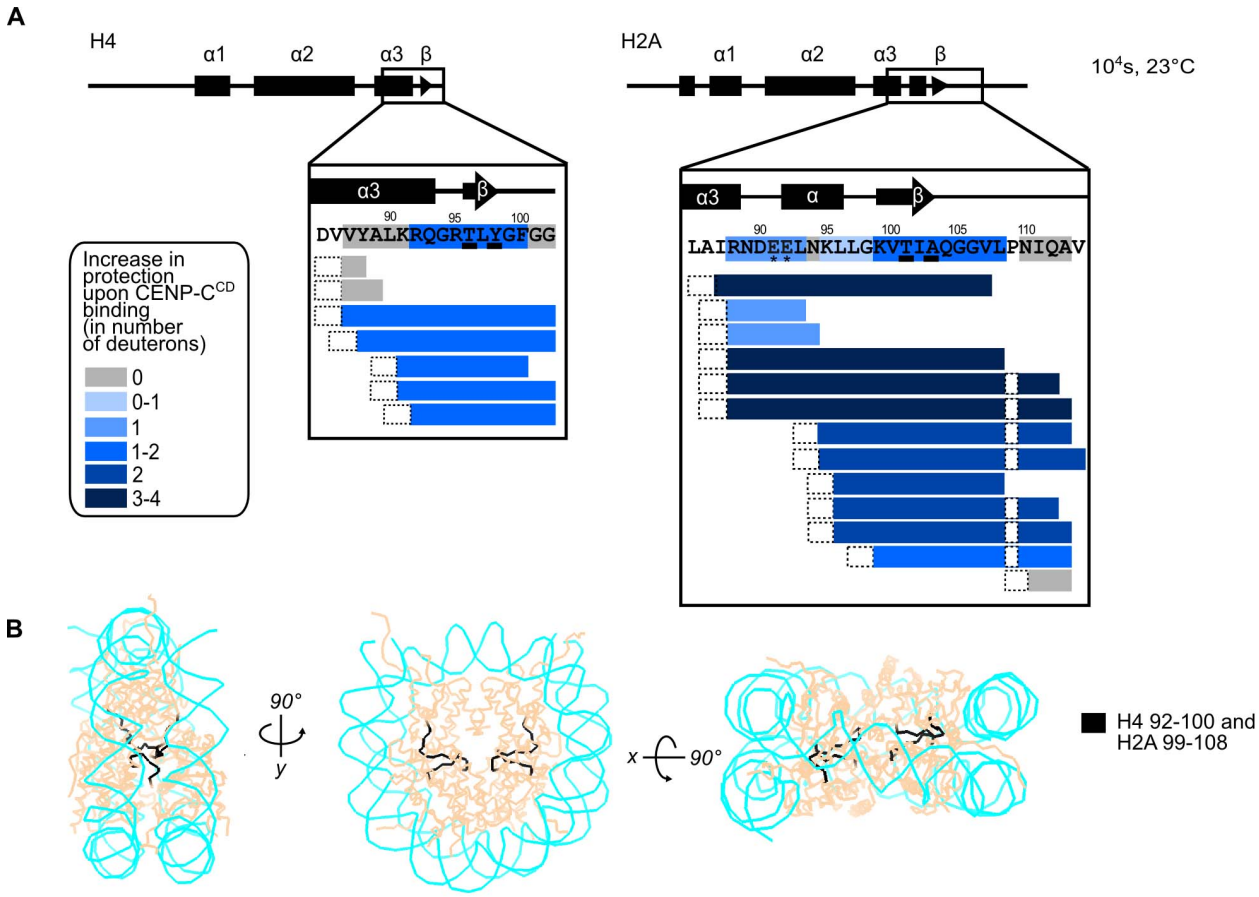

Fig. S5. Mapping HX protection in the interior of the nucleosome when CENP-C^{CD} binds to the surface of CENP-A nucleosomes.

(**A**) All peptides encompassing the β-sheet interface between H4 and H2A (the 10^4 s time point is shown) from which the minimal regions that exhibit protection is deduced to be H4 92-100 and H2A 99-108 based on partially overlapping peptide HX data. Note that protection of H2A residues encompassing the β-sheet can be distinguished from those of surface contacts (i.e., acidic patch residues marked with asterisks). Underlined residues contain the backbone amide hydrogens that engage in hydrogen bonding within the β-sheet. The first two residues of each peptide and prolines are boxed in dashed black lines because exchange of the first two backbone amide protons cannot be measured (*42*) and prolines lack amide protons. (**B**) These minimal regions are colored in black in the nucleosome structure (PDB 1KX5) and are shown in various orientations. The H2A/H4 β-sheet is buried in the interior of the nucleosome and is inaccessible to CENP-C^{CD} at the surface of the nucleosome (Figs. 2B, S4, and movie S1), so we conclude that it is stabilized concomitantly with the shape change that brings H2A/H2B dimers together.

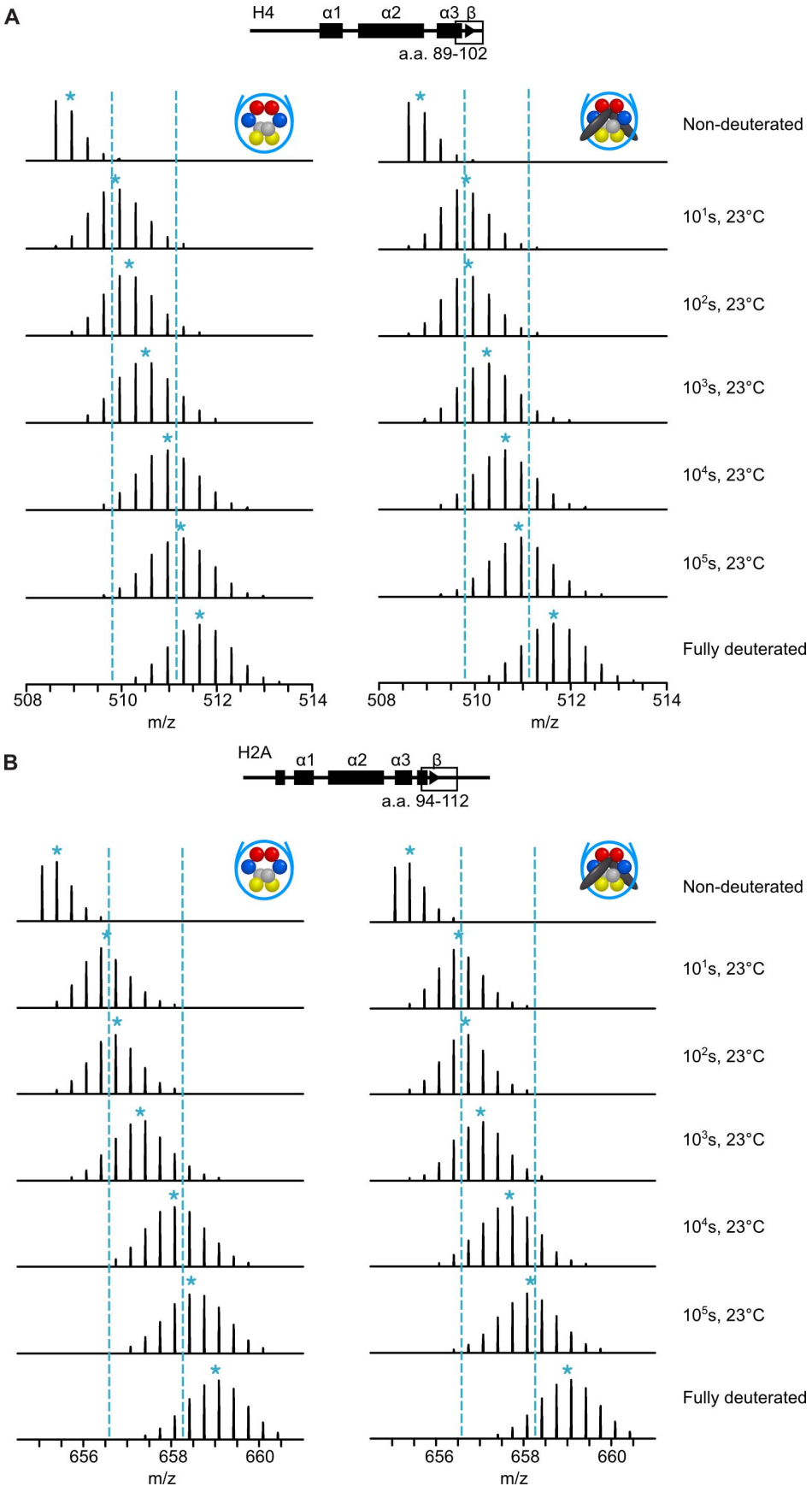
A
H4
α1
α2
α3
β
a.a. 89-102
Non-deuterated
10^1s, 23°C
10^2s, 23°C
10^3s, 23°C
10^4s, 23°C
10^5s, 23°C
Fully deuterated
508
510
512
514
m/z
B
H2A
α1
α2
α3
β
a.a. 94-112
Non-deuterated
10^1s, 23°C
10^2s, 23°C
10^3s, 23°C
10^4s, 23°C
10^5s, 23°C
Fully deuterated
656
658
660
m/z

Fig. S6. HXMS of peptides spanning the β-sheet at the interface in H4 (A) and H2A (B). In each panel, the peptide is shown from a CENP-A nucleosome (left) and a CENP-A nucleosome when in complex with CENP-C^{CD} (right). Dotted blue lines serve as guideposts to highlight the differences in m/z shifts between the two samples. A blue asterisk denotes the centroid location of each peptide envelope, and the numerical value in blue indicates the centroid mass of the peptide envelope as determined by the ExMS data analysis software (*27*).

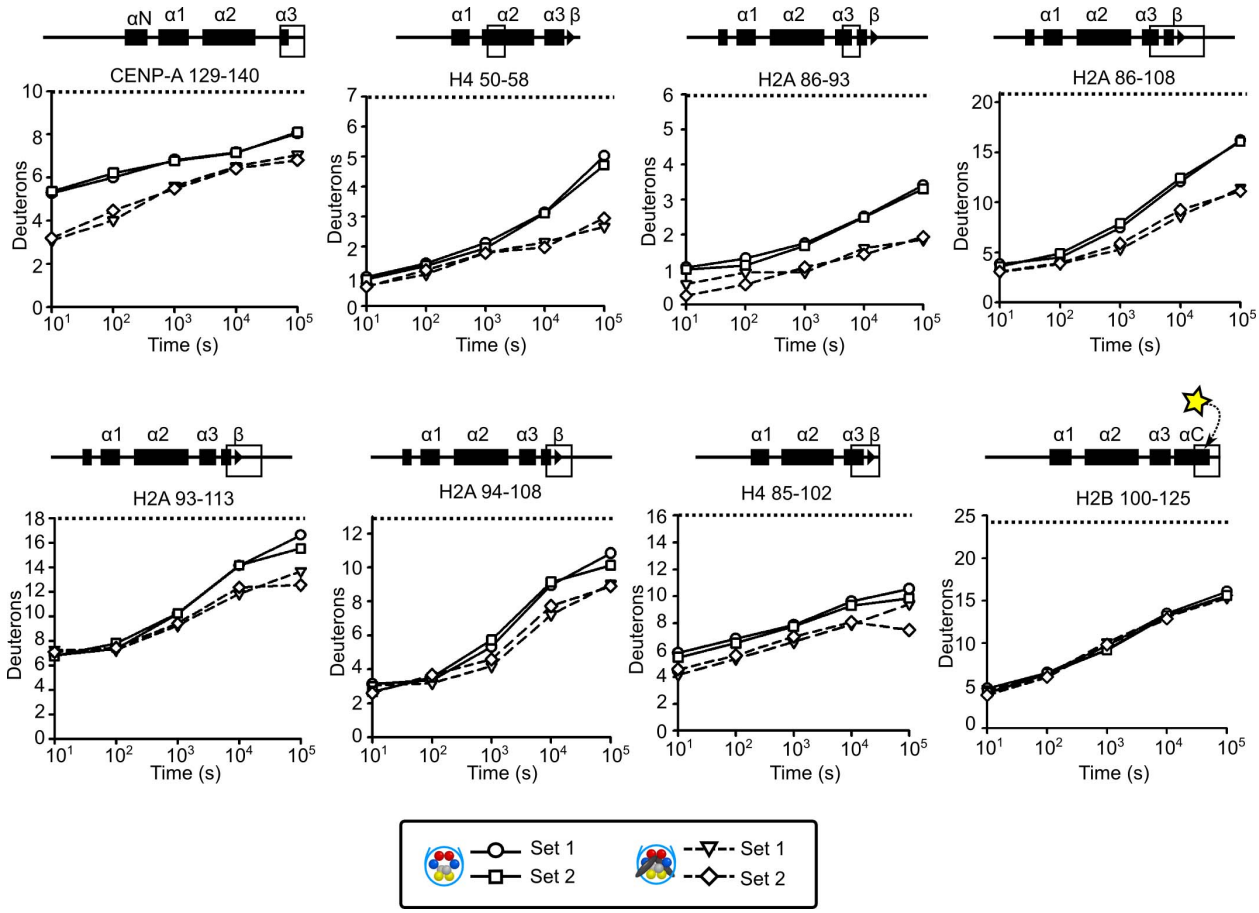

Fig. S7. Faithful detection of 1-4 deuteron differences in HXMS of CENP-A nucleosomes with and without CENP-C^{CD} bound.

The indicated peptides are compared between two replicate datasets (set 1 and 2), which represent two independent CENP-C^{CD} purifications and two entirely independent nucleosome reconstitutions. Changes of 1-2 deuterons are well within the resolution of HXMS (*40*). The star symbol in the H2B diagram indicates the position of fluorophores used in FRET experiments.

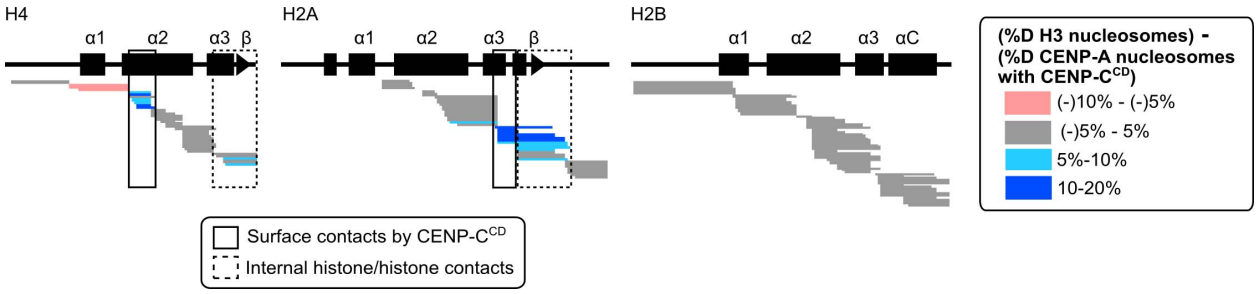

Fig. S8. Comparison of HX behavior of canonical nucleosomes to CENP-A nucleosomes bound by CENP-C^{CD}.

HXMS data with H3 nucleosomes at the 10^4 s time point showing the three histone subunits (H4, H2A, and H2B) common to the two types of nucleosomes. This is the same time point shown for CENP-A nucleosome comparisons in Fig. 2A. Peptides spanning the H4/H2A interface show protection in CENP-A nucleosomes bound to CENP-C^{CD} as compared to H3 nucleosomes, but the protection is less pronounced than the additional HX protection to CENP-A nucleosomes conferred upon binding CENP-C^{CD} (see Fig. 2A).

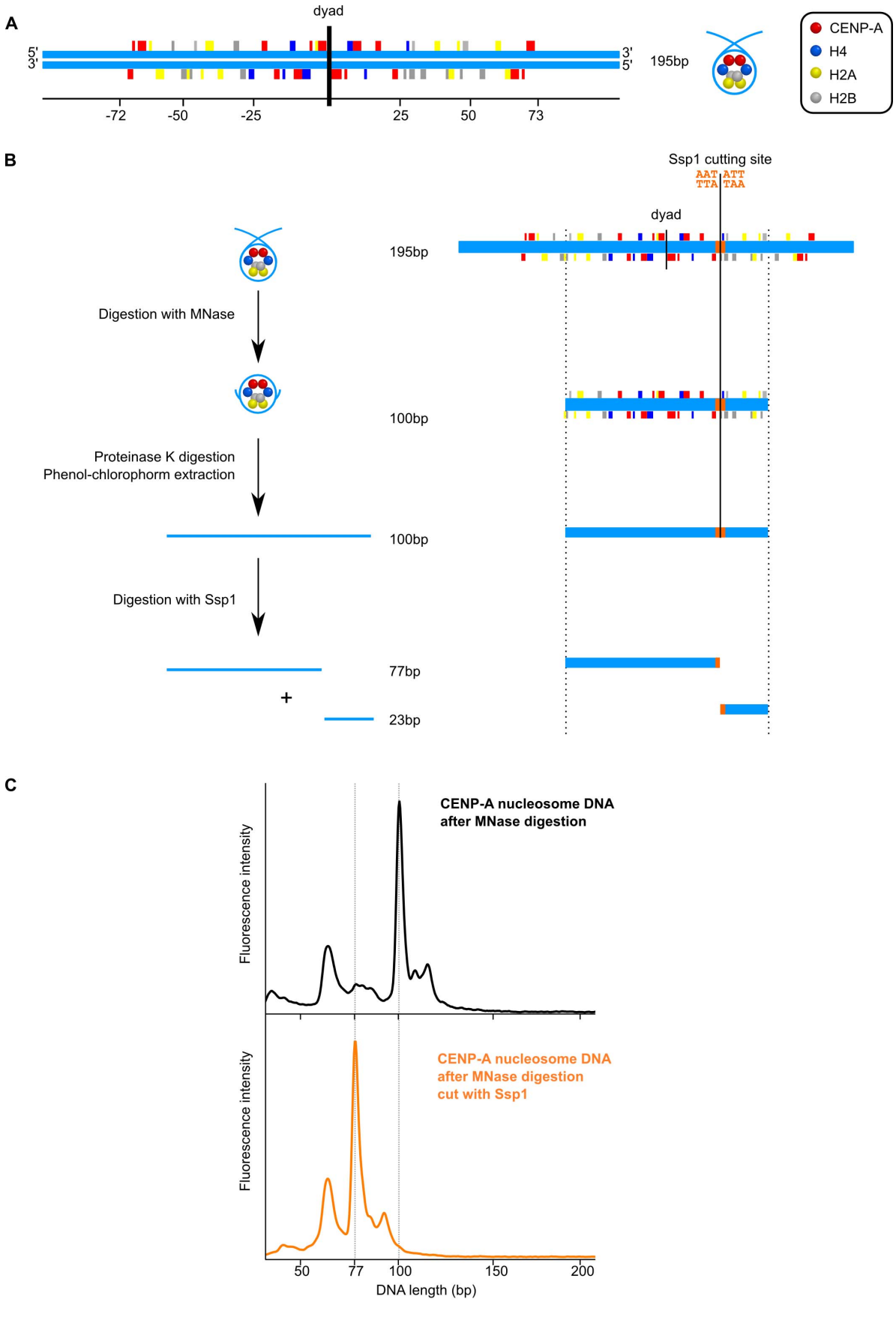
A
dyad
5'
3'
3'
5'
-72
-50
-25
25
50
73
195bp
CENP-A
H4
H2A
H2B
B
Ssp1 cutting site
AAT ATT
TTA TAA
dyad
195bp
Digestion with MNase
100bp
Proteinase K digestion
Phenol-chlorophorm extraction
100bp
Digestion with Ssp1
77bp
+
23bp
C
CENP-A nucleosome DNA
after MNase digestion
Fluorescence intensity
CENP-A nucleosome DNA
after MNase digestion
cut with Ssp1
Fluorescence intensity
50
77
100
150
200
DNA length (bp)

Fig. S9. Unique positioning and symmetric digestion to 100 bp of DNA of CENP-A nucleosomes on its native centromere sequence.
(**A**) Nucleosomal DNA (blue) with contacts between DNA and histones mapped from PDB 1AOI and 3AN2. (**B**) Schematical representation of the experiment. CENP-A nucleosomes were treated with 2 U/μg MNase and the reaction was stopped after 12 min yielding predominantly nucleosomes wrapped with 100 bp. The sample was treated with proteinase K and the DNA was isolated by phenol-chloroform extraction. The DNA was then digested with the restriction endonuclease Ssp1 (note the position of the single Ssp1 site in the 195 bp piece of nucleosomal DNA), and the resulting fragments were measured on a bioanalyzer. (**C**) Ssp1 treatment of the MNase digested nucleosomes results in a single peak of 77 bp. From the size of the fragments after Ssp1 digestion it is clear that the nucleosome is positioned symmetrically with its dyad at the precise site preferred on native human centromeres. Also, these data indicate that nucleosomes are unwrapped and digested with MNase equally from both DNA ends.

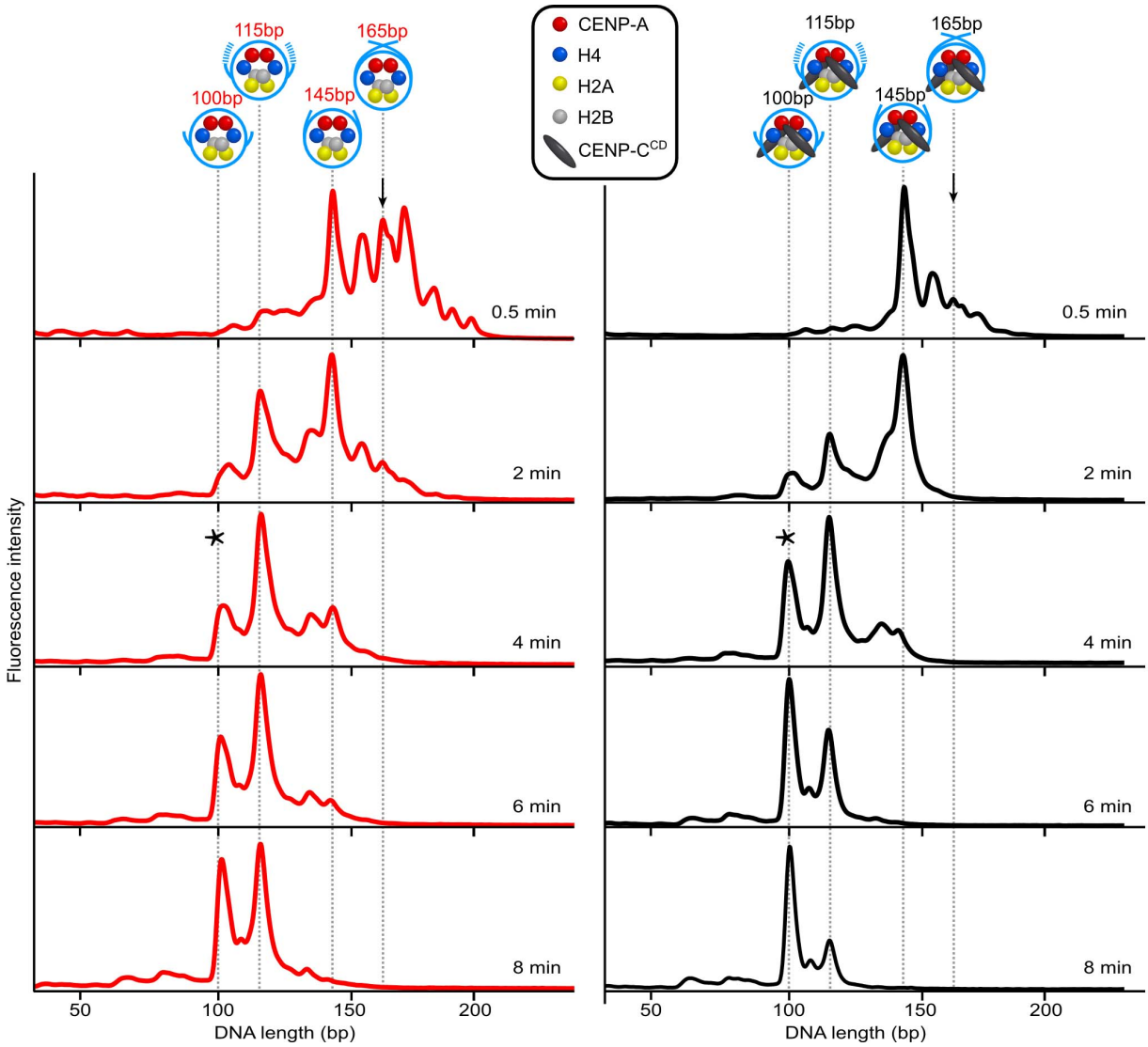

Fig. S10. Separate panels from Fig. 3B for MNase digestion profiles of CENP-A nucleosomes in the absence (red) and presence (black) of CENP-C^{CD}.

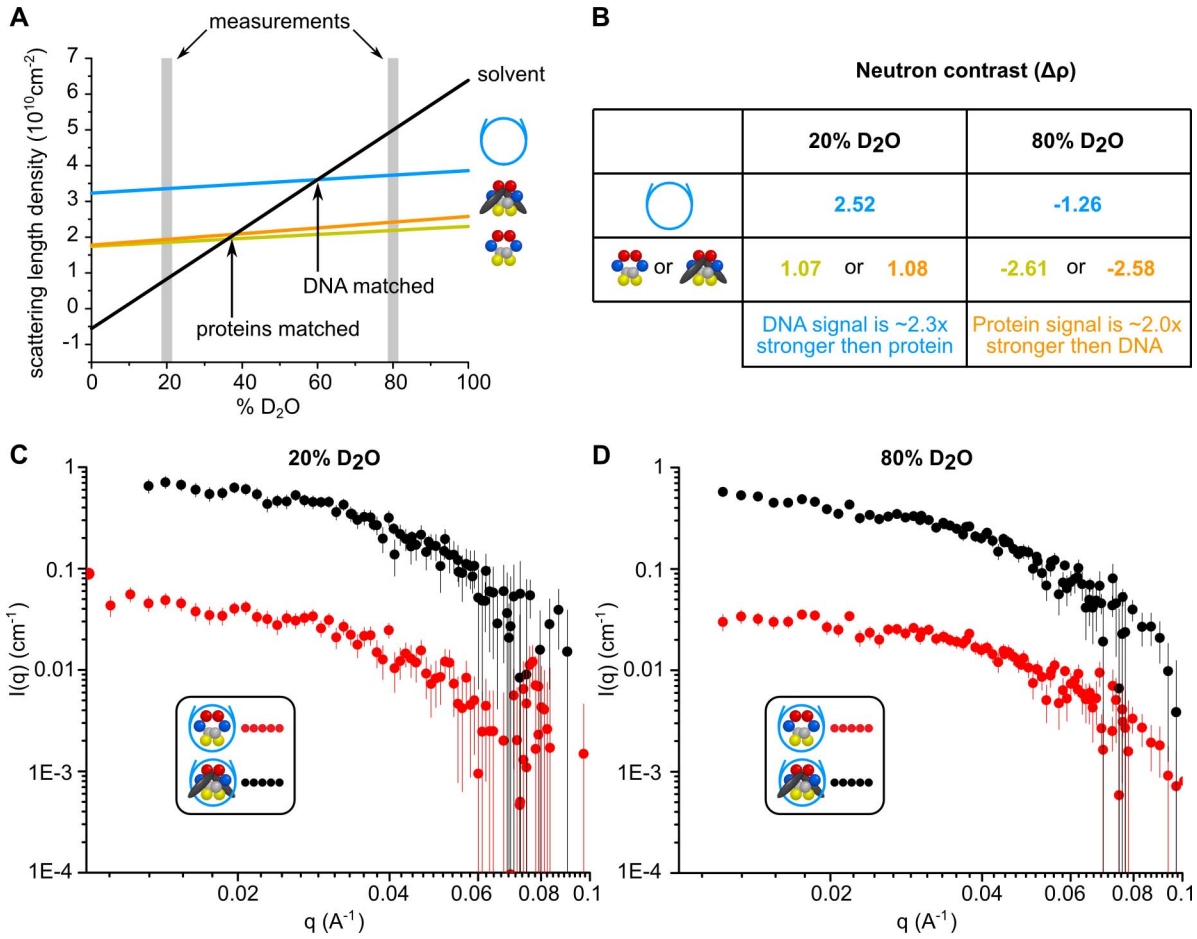

Fig. S11. SANS analysis of CENP-A nucleosomes in the presence and absence of CENP-C^{CD}.

(**A**) Variation of scattering length density is shown for solvent (black), DNA (cyan), proteins in the context of CENP-A nucleosomes (yellow) and proteins in CENP-A/CENP-C^{CD} complexes (orange). Arrows indicate contrast-matching point for DNA (60% D_2O) and proteins (37-38% D_2O). Experimental data were obtained at 20% and 80% D_2O, indicated with gray boxes. (**B**) Neutron contrasts (Δρ) calculated for DNA and protein components at 20% and 80% D_2O. The DNA signal is enhanced at 20% D_2O (~2.3x stronger than protein signal), whereas the protein signal is enhanced at 80% (~2x stronger than DNA signal). (**C**) SANS experimental solution scattering profiles of CENP-A nucleosome alone (red) and in complex with CENP-C^{CD} (black) in 20% D_2O. (**D**) SANS experimental solution scattering profiles of CENP-A nucleosome alone (red) and in complex with CENP-C^{CD} (black) in 80% D_2O.

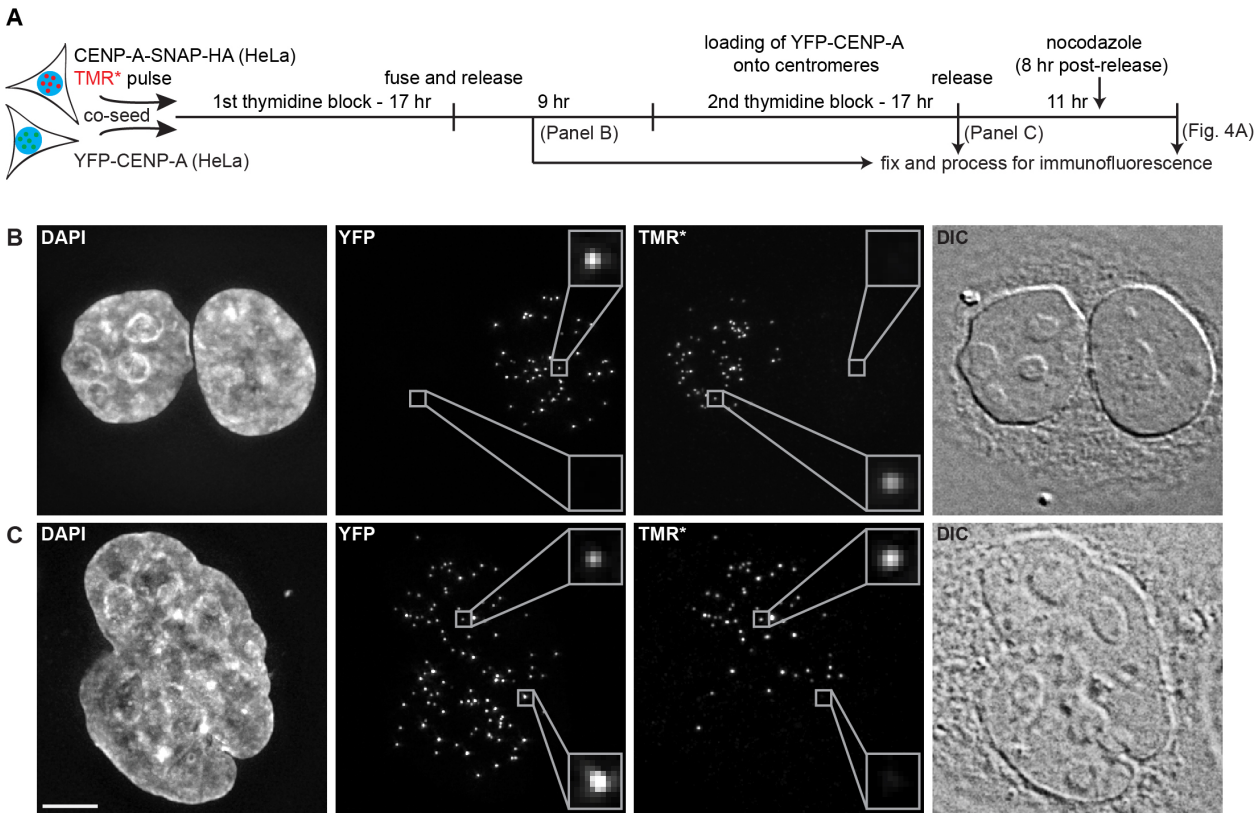

Fig. S12. Early points in centromere exchange experiments in fused cells.
(**A**) Schematic for cell fusion assay to track CENP-A stability at centromeres. The centromeric pool of CENP-A and its partner, histone H4, are not degraded in human cells over long timeframes (*11*, *16*) independently of nascent CENP-A chromatin assembly (*16*). These findings were based on pulse labeling using the SNAP-tag and monitoring the entire population at all centromeres (*11*, *16*), but monitoring the fate at *individual* centromeres over long timeframes has not been reported. *Does CENP-A exchange between centromeres during the cell cycle, or does it essentially never vacate the particular centromere upon which it was initially assembled?* The answer to this question is key to understanding the mechanisms underlying the maintenance of centromere identity, so we sought to answer it before addressing a potential role of CENP-C in stabilizing CENP-A nucleosomes (see Fig. 4). If substantial exchange occurs between centromeres after the nucleoplasm is shared, then the pulse labeled CENP-A will be distributed among all the centromeres of the fused cell. However, if negligible exchange occurs, then the pulse labeled CENP-A will be restricted to the donor centromeres. The ultimate time point in this experiment is key because the appearance of sister centromeres provides unequivocal evidence that the underlying centromere DNA duplicated in the previous S-phase, but the TMR* signal remained with donor centromeres (Fig. 4A). By monitoring the fate of CENP-A at individual centromeres over an entire cell cycle, our findings extend upon and support earlier conclusions based on the lack of recovery from photobleaching of fluorescently tagged CENP-A during 3-4 hour intervals at points in the cell cycle outside of early G1 (*43*). (**B**) Representative image of a fused cell containing YFP-tagged and SNAP-tagged CENP-A labeled with TMR* 4 hours post-fusion. This is prior to the first mitosis after fusion. (**C**) Representative image of a fused cell containing YFP-tagged and SNAP-tagged CENP-A labeled with TMR* at the first G1/S transition with a shared nucleoplasm. In each panel, the left image shows DNA, the middle two

images show the donor and acceptor fluorophore channels, respectively, and the right image shows differential interference contrast (DIC). Note the shared cytoplasm in the DIC channel in (B). Insets are 3x magnified views of the boxed area. Scale bar = 5 μm.

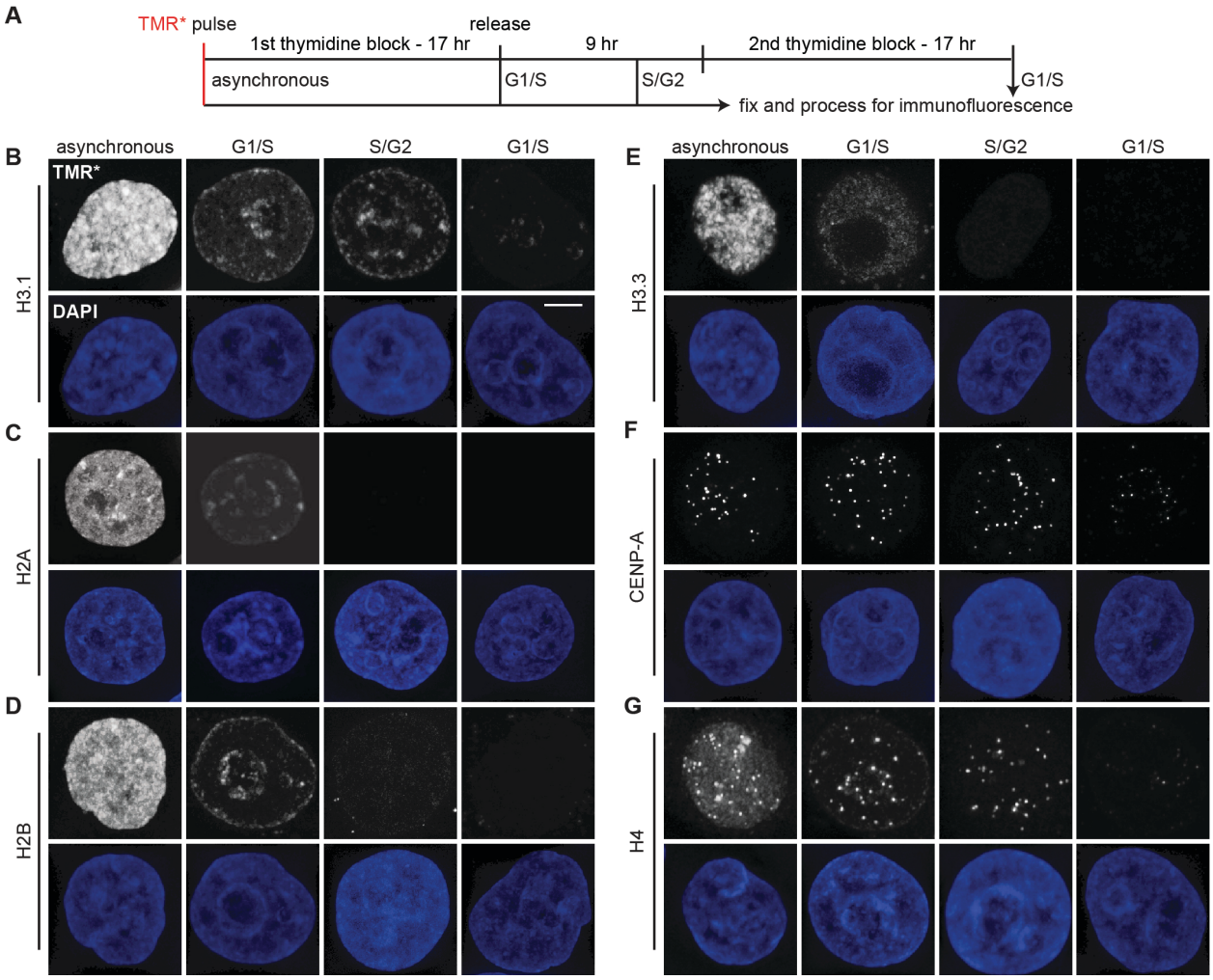

Fig. S13. Only the centromeric pool of H4 is retained in chromatin long enough to detect in our cell fusion experiments that span an entire cycle with a shared nucleoplasm.
(**A**) Schematic for TMR* SNAP labeling assay to track histone turnover in HeLa cells. (**B** to **G**), Representative maximum projected fluorescence images of TMR* labeled SNAP-tagged histones in HeLa cells. H3.1 (B), H2A (C), H2B (D), and H3.3 (E) turn over more rapidly than CENP-A (F) or H4 (G), as seen by their marked decrease in signal by S/G2, and thus turn over too quickly to monitor over the duration of our cell fusion experimental scheme. Note that for early time points, H3.1, H2A, and H2B levels are maintained in heterochromatic regions (near nuclear periphery and nucleoli) but are still essentially turned over by the second G1/S phase, unlike CENP-A and H4. Scale bar = 5 μm.

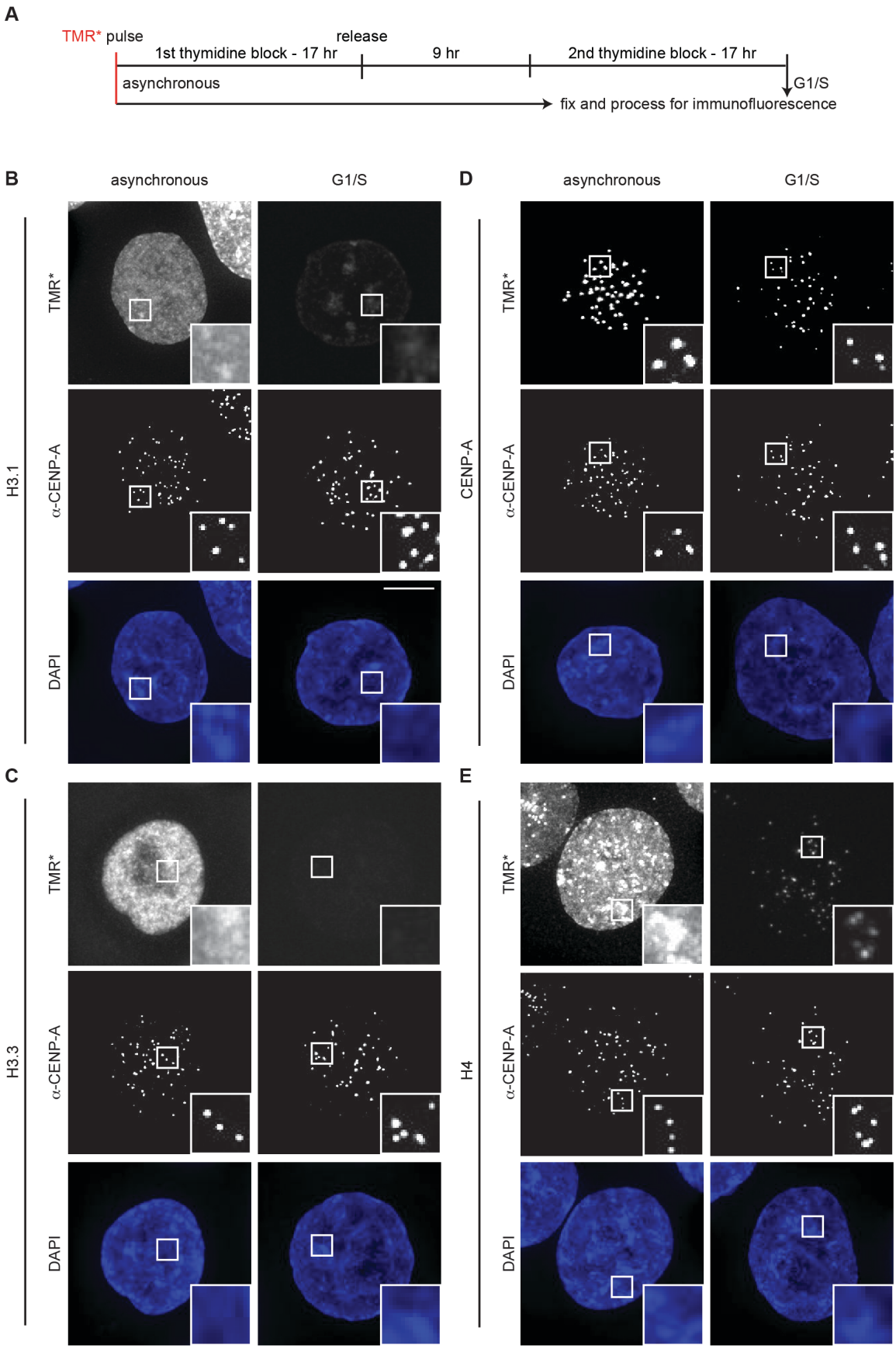
A
TMR* pulse
release
1st thymidine block - 17 hr
9 hr
2nd thymidine block - 17 hr
asynchronous
G1/S
fix and process for immunofluorescence
B
asynchronous
G1/S
H3.1
TMR*
α-CENP-A
DAPI
C
H3.3
TMR*
α-CENP-A
DAPI
D
asynchronous
G1/S
CENP-A
TMR*
α-CENP-A
DAPI
E
H4
TMR*
α-CENP-A
DAPI

Fig. S14. Only CENP-A and H4 are retained at centromeres in our TMR* SNAP assays, while a small amount of H3.1 is retained at an adjacent chromatin location.
(**A**) Schematic for TMR* SNAP labeling assay to track histone colocalization with the centromere in HeLa cells. (**B-E**), Representative maximum projected fluorescence images of TMR* labeled SNAP-tagged histones in HeLa cells. H3.1 (B) and H3.3 (C) do not colocalize with centromeres at the final time point analyzed, while CENP-A (D) and H4 (E) colocalize, as seen by overlap with α-CENP-A staining. Additionally, essentially all H3.3 is turned over at the final time point, while the remaining H3.1 is adjacent to—but does not directly overlap with—α-CENP-A staining, suggesting that the small amount of H3.1 that is retained resides in pericentromeric regions. Insets are 3x magnification. Scale bar = 5 μm.

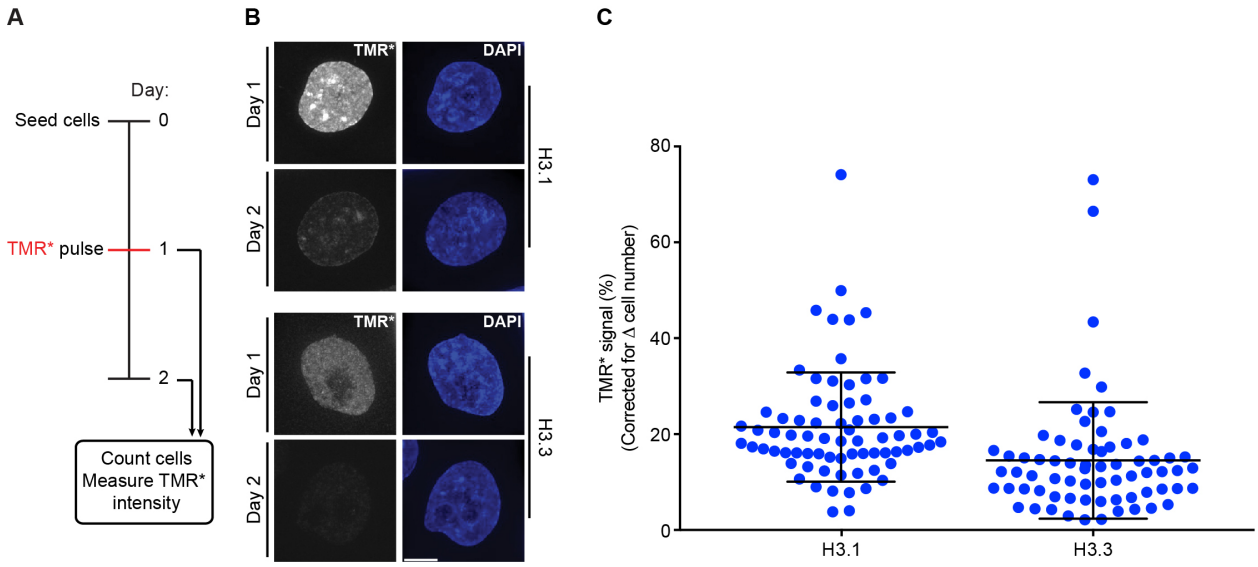

Fig. S15. H3.1 and H3.3 turn over rapidly.
(**A**) Schematic for tracking H3.1 and H3.3 levels after a 24 hour period. (**B**) Cells were pulse labeled with TMR* (Day 1) and the relative H3.1 and H3.3 signals were analyzed (Day 2). Scale bar = 5 μm. (**C**) Quantification of H3.1 and H3.3 signal retained at day 2, adjusted to reflect the total pool of labeled H3 by accounting for the increase in cell number in the dividing cell populations following TMR* pulse. N = 65-75 cells.

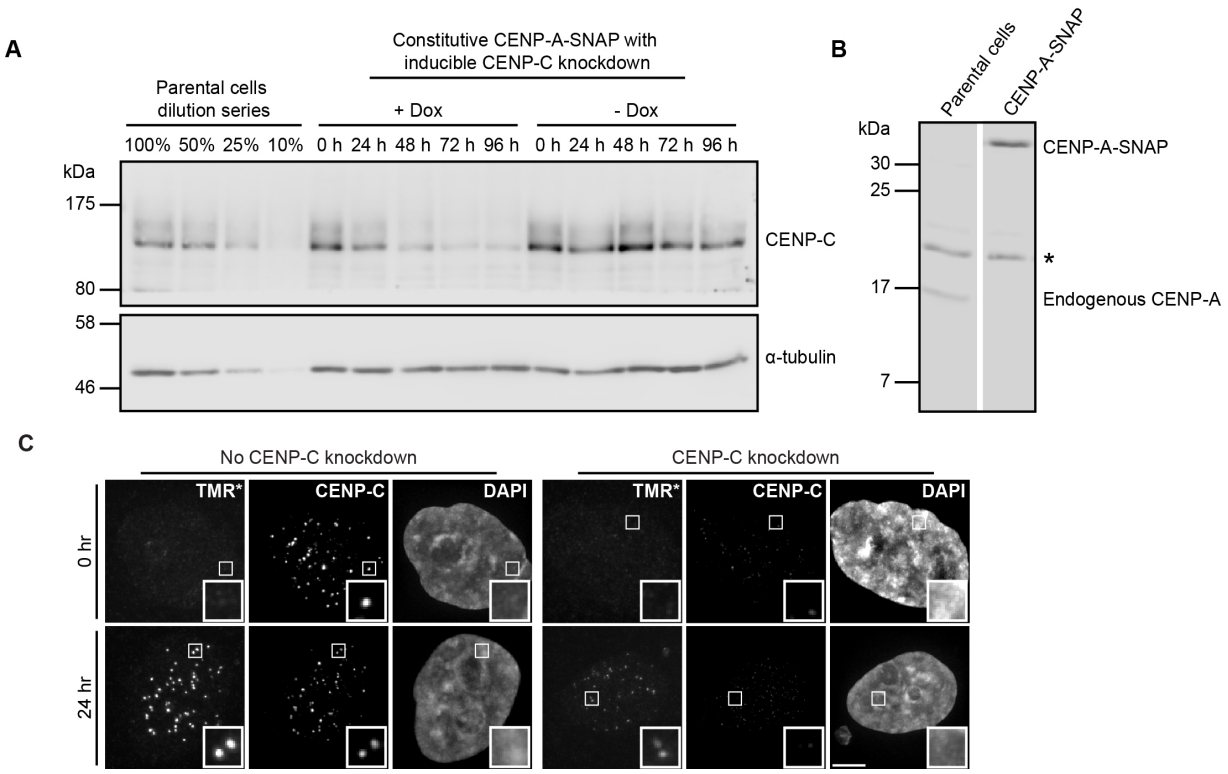

Fig. S16. CENP-C knockdown effects on retention and assembly of CENP-A at the centromere.

(**A**) Immunoblot of CENP-C levels in inducible CENP-C knockdown cells at indicated timepoints after Dox addition, compared to the cells without Dox. Whole cell lysate dilutions from parental cells were used to measure the extent of CENP-C knockdown. α-tubulin levels were used as a loading control. CENP-C depletion requires several days prior to when cell death occurs (Fig. 4F) following mitotic kinetochore failure (*44*), so there is an experimental window of time in which we can test if CENP-A nucleosome retention persists after the majority of CENP-C protein has been depleted (Figs. 4F,G). SNAP labeling of the existing pool of CENP-A (Fig. 4G [Day 2]) combined with monitoring cell number allows one to account for the entire pool of CENP-A in the dividing cell population during the course of the experiment (*16*). This approach also overcomes the limitation of the CENP-A-PAGFP approach (Fig. 4D) where measurements beyond ~8 hr become problematic due to cell divisions. (**B**) Immunoblot of CENP-A levels in parental and CENP-A-SNAP cell lines. Asterisk denotes non-specific band. (**C**) We performed a quench-chase-pulse experiment where cells were synchronized using a double-thymidine block, pre-existing CENP-A was quenched with a non-fluorescent label, and the nascent pool of CENP-A was pulse-labeled with TMR* 6.5 hours post-release just prior to loading. Left, representative maximum projected immunofluorescence images of CENP-A-SNAP cells. Right, representative images of CENP-A-SNAP + CENP-C knockdown cells. Insets are a 3x magnification of selected representative centromeres. Scale bar = 5 μm.

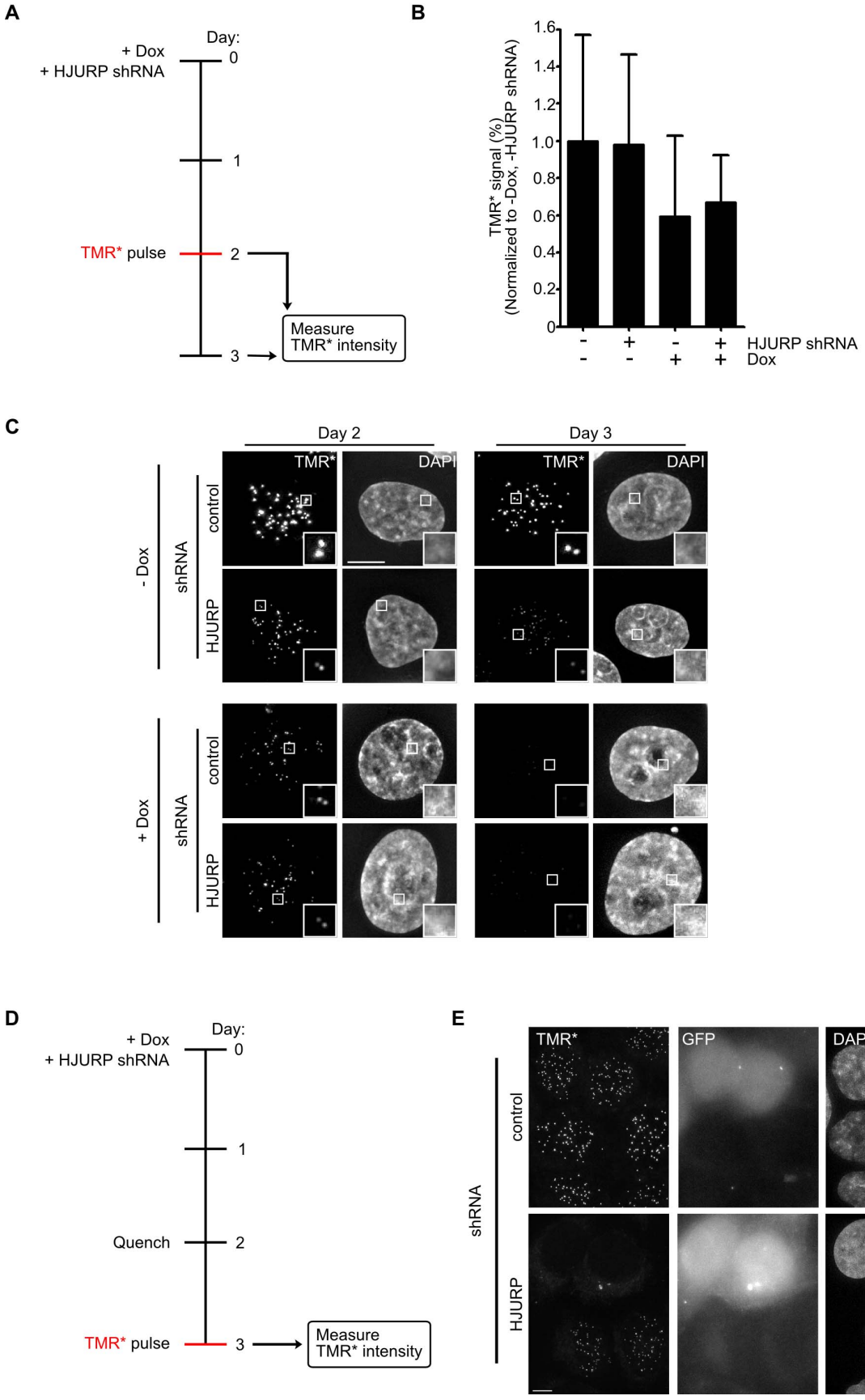
A
Day:
+ Dox
+ HJURP shRNA
0
1
TMR* pulse
2
Measure
TMR* intensity
3
B
TMR* signal (%)
(Normalized to -Dox, -HJURP shRNA)
1.6
1.4
1.2
1.0
0.8
0.6
0.4
0.2
0
HJURP shRNA
Dox
C
Day 2
Day 3
TMR*
DAPI
- Dox
+ Dox
shRNA
control
HJURP
D
Day:
+ Dox
+ HJURP shRNA
0
1
Quench
2
TMR* pulse
3
Measure
TMR* intensity
E
TMR*
GFP
DAPI
shRNA
control
HJURP

Figure S17. The reduction of CENP-A retention upon CENP-C knockdown is independent of new CENP-A chromatin assembly.

To determine whether CENP-C knockdown could reduce centromeric CENP-A levels in the absence of new CENP-A assembly, we quantified CENP-A retention upon co-depletion of CENP-C and HJURP. (**A**) Schematic of pulse-chase experiment to track CENP-A levels, combined with knockdown of both CENP-C and HJURP. Cells with (+ Dox) and without (- Dox) CENP-C depletion were co-transfected with shRNA-encoding plasmid targeting nucleotides 1288-1306 of HJURP (pSRP-HJURP) (*45*) or the control plasmid (pSRP). A plasmid encoding GFP was co-transfected at a 9:1 (shRNA:GFP) ratio to mark transfected cells. The cells were pulse-labeled with TMR* (Day 2) and the CENP-A-SNAP signals were analyzed at day 2 and 3. (**B**) Quantification of CENP-A-SNAP signal retained at day 3. For each condition, >700 centromeres in GFP-positive cells were quantitated using the Centromere Recognition and Quantitation macro (37) in ImageJ, and each TMR* value at day 3 was divided by its average TMR* value at day 2, then normalized to the - Dox, mock-transfected condition and plotted as mean ± s.d. (**C**) Representative images of GFP positive cells. CENP-C knockdown upon dox treatment was confirmed separately. Insets are 3x magnification. (**D**) We performed a quench-chase-pulse experiment on the same transfected cells used for panels A-C to assess whether or not the HJURP knockdown compromised new CENP-A assembly. By quenching pre-existing CENP-A with a non-fluorescent substrate and performing the TMR* labeling after 24 hours, we exclusively examine the pool of CENP-A-SNAP that had been newly synthesized and loaded onto centromeres. We TMR* labeled immediately after quenching and confirmed the lack of detectable TMR* signal in all conditions. (**E**) Representative images showing that transfection of HJURP shRNA abolishes new CENP-A loading. Note the assembly of CENP-A in the untransfected cells (GFP negative) adjacent to those that received HJURP shRNAs (GFP positive). Scale bars = 5 μm.

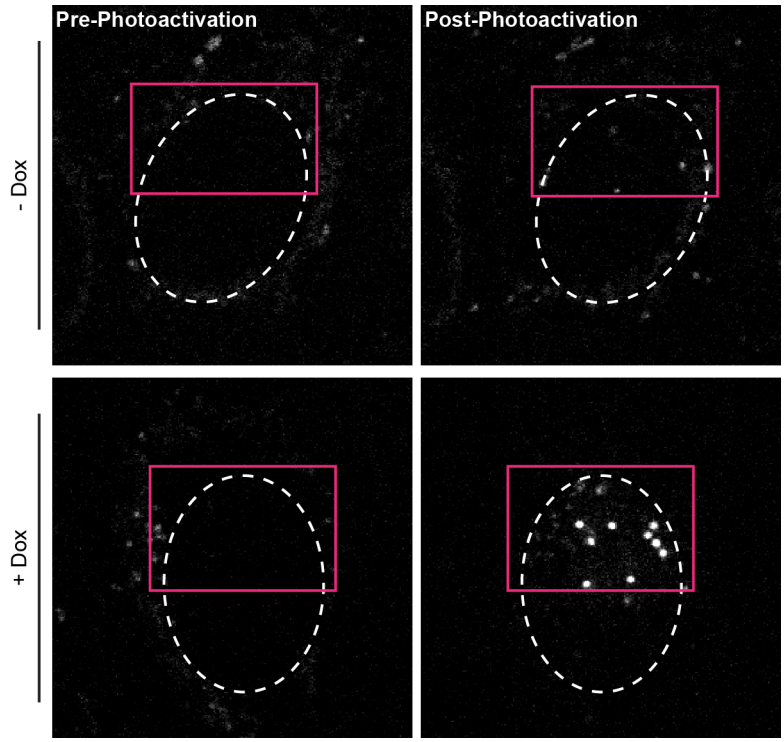

Fig. S18. Levels of CENP-A-PAGFP overexpression are doxycycline-dependent. Representative images of cells treated with or without 50 ng/mL of dox for 48 hr and then immediately photoactivated. Pink boxes denote the photoactivated region and white dotted lines denote the nucleus. Note that at 50 ng/mL of dox does not result in the same level of CENP-A expression as seen in Fig. 4D where 20x [Dox] is used.

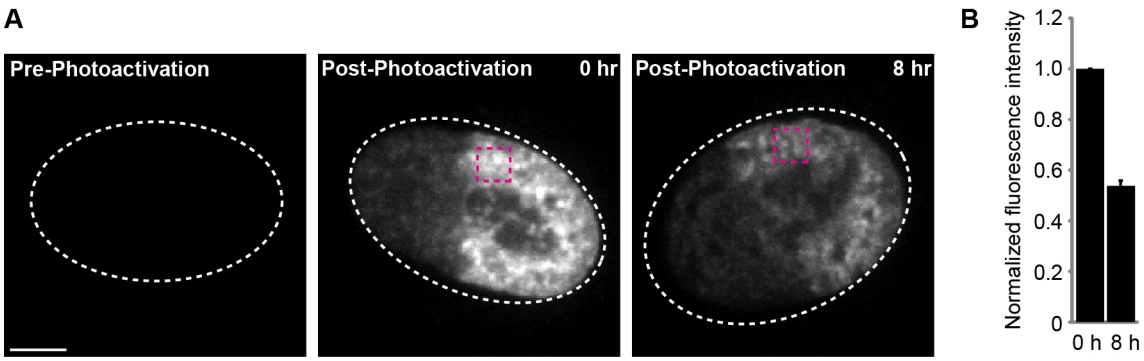

Fig. S19. Measuring the turnover of H3.1.
(**A**) Representative image of experiment with H3.1-PAGFP photoactivation in a section of the nucleus. Pink box defines a representative ROI selected for quantification. Note that the images show a single z-section through the nucleus. Scale bar = 5 μm. (**B**) Quantification of experiment in (**A**). Data shown as mean ± s.e.m.

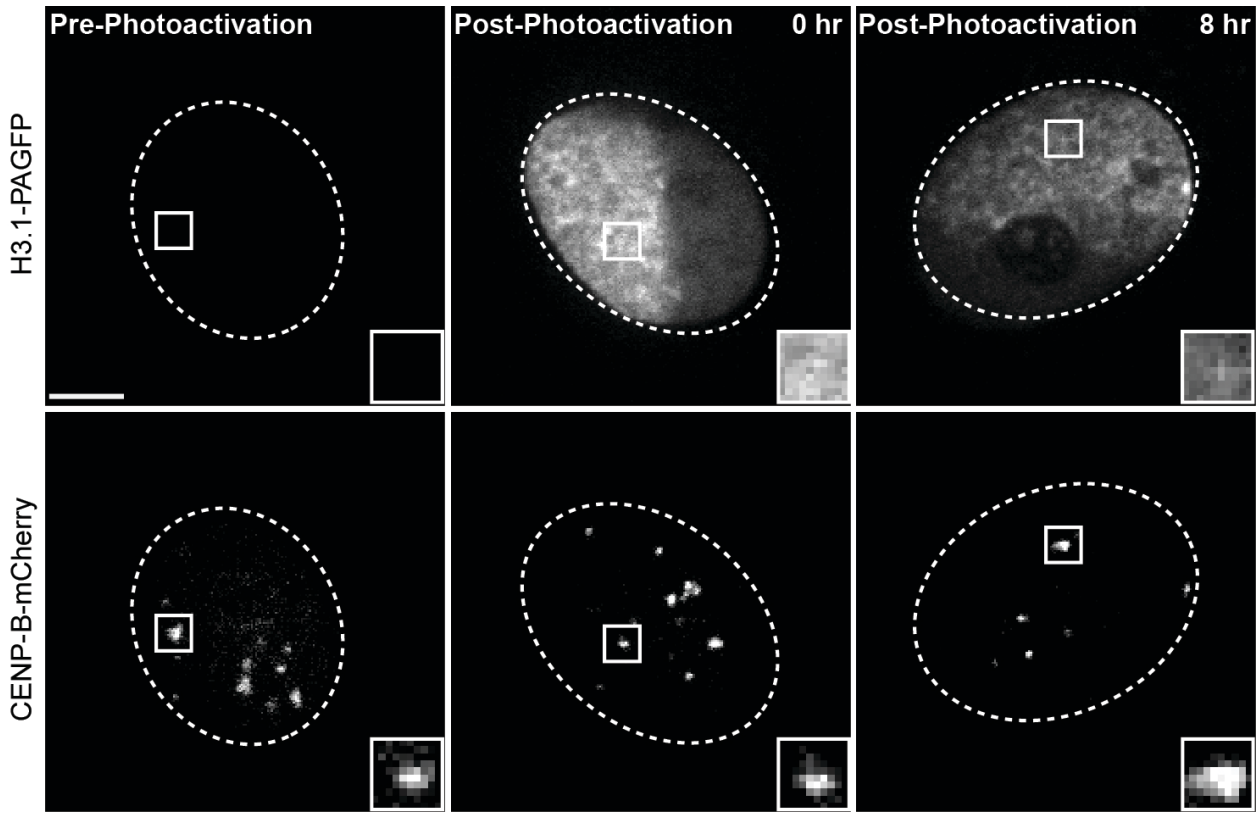

Fig. S20. H3.1 is not strongly retained at centromeres.
HeLa cells constitutively expressing H3.1-PAGFP and transfected with a plasmid encoding CENP-B-mCherry (*46*). H3.1-PAGFP near the centromere is slightly more intense both before and after an 8 hr incubation following photoactivation. Insets are 2x magnification. Scale bar = 5 μm.

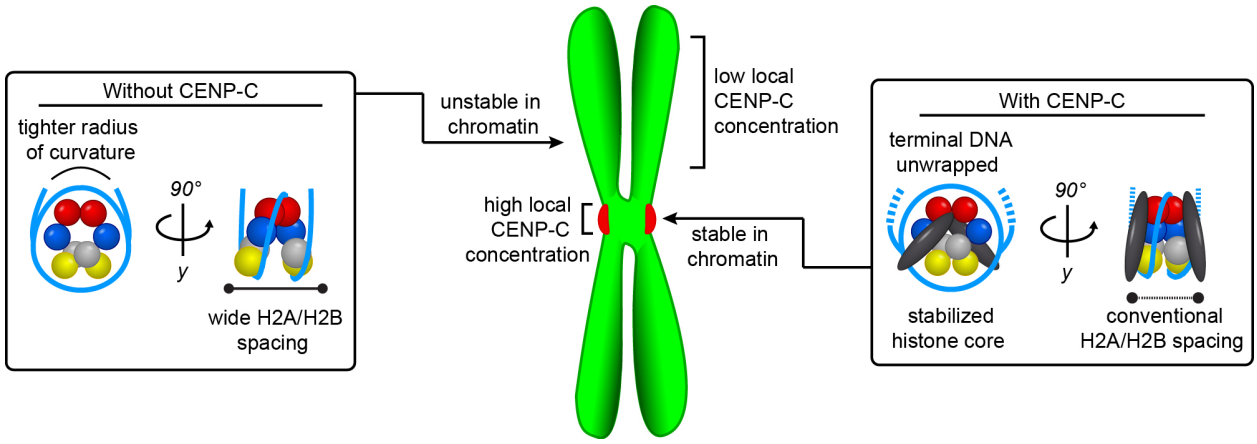

Fig. S21. Summary model for collaboration of CENP-C with CENP-A nucleosomes in specifying centromere location.

At the centromere, there is a high local concentration of CENP-A, which results in a high local concentration of CENP-C. Together, CENP-A and CENP-C collaborate to form a stable complex that maintains the epigenetic mark of the centromere. In the chromatin arms, CENP-A levels do not reach a sufficient threshold to recruit CENP-C and CENP-A is quickly turned over. Our experiments support the idea that CENP-A-containing nucleosomes prefer an atypical shape in the absence of CENP-C, but adopt a conventional overall histone octamer shape when CENP-C binds. In addition, our reconstitutions on native centromere DNA of octameric CENP-A nucleosomes very closely match the DNA wrapping properties of CENP-A nucleosomes isolated from functional human centromeres (*7*), especially when CENP-C is bound (Fig. 3B). This is in stark contrast to half-nucleosomes (termed hemisomes; i.e. one copy each of CENP-A, H4, H2A, and H2B) that wrap 65 bp of DNA (*47*) and have been proposed by others to be the major form at centromeres (*48*, *49*). Importantly, until now CENP-C has been considered primarily as a protein that recognizes CENP-A and bridges centromeric chromatin to other proteins important for centromere and kinetochore function (*2*, *3*, *12*, *50–53*) and helping target new CENP-A chromatin assembly at the centromere each cell cycle (*12, 13*), but our findings that its binding directs changes to the shape and dynamics of the nucleosome suggest that it could also play a role in the special stability of CENP-A at centromeres *in a manner analogous to allosteric regulation of enzymes*. This has potential implications for chromatin regulation at diverse chromosome locations, as such a feature has not been reported for some other non-catalytic nucleosome binding proteins studied to date, like RCC1 and Sir3 (*54*, *55*), but now is worth considering for these and other nucleosome binding proteins. Directing a structural change upon binding of one component to a macromolecular complex to alter its behavior is a general strategy in biology, and our work with CENP-C importantly illustrates that a nucleosome—*in this case, the special type at the centromere*—is no exception.

Table S1. Anisotropy measurements for nucleosomes labeled with C343 and RhB. Anisotropy values were measured for both C343 and RhB fluorophores attached to histone H2B in the indicated C343-RhB-containing nucleosomes (See Methods and figs. S1 and S2). Note that all values are below 0.2, indicating that the fluorophores are freely rotating in solution. Thus, using $\kappa^2 = 2/3$ as an estimate in calculating R_0 is a valid assumption.

	Anisotropy	
	Coumarin 343	**Rhodamine B**
H3 nucleosomes	0.087 ± 0.004	0.107 ± 0.008
CENP-A nucleosomes	0.102 ± 0.004	0.117 ± 0.009
CENP-A nucleosomes + CENP-C^{CD}	0.148 ± 0.002	0.128 ± 0.007

Table S2. Lifetime measurements of nucleosomes labeled with C343 and RhB.
Reported lifetimes of C343 for the indicated C343-RhB-containing nucleosomes. Lifetimes were calculated by fitting raw data to two-exponential fits because FRET samples contain both C343-RhB and C343-only nucleosomes (See Methods and figs. S1 and S2). The first exponential term is fixed to have a lifetime of 4.22 ns, which is representative of the measured lifetime of C343 in C343-only nucleosome for all three nucleosome types. The other fitted exponential term determines the measured lifetime of C343 in C343-RhB nucleosomes. The lifetime of C343 (the donor fluorophore) decreases in the presence of RhB (the acceptor fluorophore) and this decrease in lifetime is proportional to FRET efficiency. Note that CENP-A nucleosomes have the longest measured lifetime, indicative of the lowest FRET efficiency of all three samples. This is consistent with the direction and magnitude of the distance changes that we calculated from the steady-state efficiency measurements in Fig. 1.

	Lifetime (ns)
H3 nucleosomes	2.02 ± 0.11
CENP-A nucleosomes	2.36 ± 0.13
CENP-A nucleosomes + CENP-C^{CD}	2.00 ± 0.06

Table S3. Extended table of parameters for SANS measurements.
Parameters derived from SANS analysis of CENP-A nucleosomes and CENP-A nucleosomes in complex with CENP-C^{CD}. Contrast variation exploits the difference between D_2O and H_2O in neutron scattering, and allows one to measure the size and shape of a protein/DNA complex in conditions where the overall scattering is dominated by the DNA (i.e. at 20% D_2O) or by the protein (i.e. at 80% D_2O). This method provided the earliest proof that nucleosomal DNA is wrapped around histones (and not vice versa) as the DNA-dominated SANS dimensions are larger (*56*). Results derived from Guinier analyses are in concordance with those derived from the inverse Fourier transform (GNOM).

			Guinier analysis			GNOM analysis			
	D_2O	**Conc** (mg/mL)	**qR_g**	**R_g** (Å)	**I(0)** (cm^{-1})	**Q**	**R_g** (Å)	**I(0)** (cm^{-1})	**D_{max}** (Å)
CENP-A nucleosomes	20%	2.0	0.57 - 1.28	42.3 ± 6.4	0.048 ± 0.005	0.009 - 0.011	42.3 ± 2.6	0.0465	123
	80%	1.0	0.64 - 1.42	38.8 ± 3.2	0.037 ± 0.003	0.009 - 0.12	38.4 ± 1.0	0.0349	112
CENP-A nucleosomes + CENP-C^{CD}	20%	1.5	0.58 - 1.61	43.9 ± 2.9	0.075 ± 0.005	0.009 - 0.16	44.0 ± 2.2	0.0732	130
	80%	1.0	0.55 - 1.54	41.4 ± 1.7	0.053 ± 0.002	0.009 - 0.16	41.2 ± 0.8	0.0511	117

Movie S1. Regions on the surface and interior of the CENP-A nucleosome that exhibit additional substantial protection from HX upon CENP-C^{CD} binding, colored onto the solvent-accessible surface representation of the CENP-A nucleosome structure (PDB 3AN2), with solvent radius of 1.4 Å.

References

1. B. E. Black, D. W. Cleveland, Epigenetic centromere propagation and the nature of CENP-a nucleosomes. *Cell* **144**, 471–479 (2011). Medline doi:10.1016/j.cell.2011.02.002

2. C. W. Carroll, K. J. Milks, A. F. Straight, Dual recognition of CENP-A nucleosomes is required for centromere assembly. *J. Cell Biol.* **189**, 1143–1155 (2010). Medline doi:10.1083/jcb.201001013

3. H. Kato, J. Jiang, B. R. Zhou, M. Rozendaal, H. Feng, R. Ghirlando, T. S. Xiao, A. F. Straight, Y. Bai, A conserved mechanism for centromeric nucleosome recognition by centromere protein CENP-C. *Science* **340**, 1110–1113 (2013). Medline doi:10.1126/science.1235532

4. H. Tachiwana, W. Kagawa, T. Shiga, A. Osakabe, Y. Miya, K. Saito, Y. Hayashi-Takanaka, T. Oda, M. Sato, S. Y. Park, H. Kimura, H. Kurumizaka, Crystal structure of the human centromeric nucleosome containing CENP-A. *Nature* **476**, 232–235 (2011). Medline doi:10.1038/nature10258

5. K. Luger, A. W. Mäder, R. K. Richmond, D. F. Sargent, T. J. Richmond, Crystal structure of the nucleosome core particle at 2.8 A resolution. *Nature* **389**, 251–260 (1997). Medline doi:10.1038/38444

6. N. Sekulic, E. A. Bassett, D. J. Rogers, B. E. Black, The structure of $(CENP\text{-}A\text{-}H4)_2$ reveals physical features that mark centromeres. *Nature* **467**, 347–351 (2010). Medline doi:10.1038/nature09323

7. D. Hasson, T. Panchenko, K. J. Salimian, M. U. Salman, N. Sekulic, A. Alonso, P. E. Warburton, B. E. Black, The octamer is the major form of CENP-A nucleosomes at human centromeres. *Nat. Struct. Mol. Biol.* **20**, 687–695 (2013). Medline doi:10.1038/nsmb.2562

8. P. T. Lowary, J. Widom, New DNA sequence rules for high affinity binding to histone octamer and sequence-directed nucleosome positioning. *J. Mol. Biol.* **276**, 19–42 (1998). Medline doi:10.1006/jmbi.1997.1494

9. J. M. Harp, E. C. Uberbacher, A. E. Roberson, E. L. Palmer, A. Gewiess, G. J. Bunick, X-ray diffraction analysis of crystals containing twofold symmetric nucleosome core particles. *Acta Crystallogr. D Biol. Crystallogr.* **52**, 283–288 (1996). Medline doi:10.1107/S0907444995009139

10. R. D. Kornberg, Structure of chromatin. *Annu. Rev. Biochem.* **46**, 931–954 (1977). Medline doi:10.1146/annurev.bi.46.070177.004435

11. L. E. T. Jansen, B. E. Black, D. R. Foltz, D. W. Cleveland, Propagation of centromeric chromatin requires exit from mitosis. *J. Cell Biol.* **176**, 795–805 (2007). Medline doi:10.1083/jcb.200701066

12. S. Erhardt, B. G. Mellone, C. M. Betts, W. Zhang, G. H. Karpen, A. F. Straight, Genome-wide analysis reveals a cell cycle-dependent mechanism controlling centromere propagation. *J. Cell Biol.* **183**, 805–818 (2008). Medline doi:10.1083/jcb.200806038

13. B. Moree, C. B. Meyer, C. J. Fuller, A. F. Straight, CENP-C recruits M18BP1 to centromeres to promote CENP-A chromatin assembly. *J. Cell Biol.* **194**, 855–871 (2011). Medline

14. E. A. Bassett, J. DeNizio, M. C. Barnhart-Dailey, T. Panchenko, N. Sekulic, D. J. Rogers, D. R. Foltz, B. E. Black, HJURP uses distinct CENP-A surfaces to recognize and to stabilize CENP-A/histone H4 for centromere assembly. *Dev. Cell* **22**, 749–762 (2012). Medline doi:10.1016/j.devcel.2012.02.001

15. B. E. Black, D. R. Foltz, S. Chakravarthy, K. Luger, V. L. Woods Jr., D. W. Cleveland, Structural determinants for generating centromeric chromatin. *Nature* **430**, 578–582 (2004). Medline doi:10.1038/nature02766

16. D. L. Bodor, L. P. Valente, J. F. Mata, B. E. Black, L. E. T. Jansen, Assembly in G1 phase and long-term stability are unique intrinsic features of CENP-A nucleosomes. *Mol. Biol. Cell* **24**, 923–932 (2013). Medline doi:10.1091/mbc.E13-01-0034

17. P. N. Dyer, R. S. Edayathumangalam, C. L. White, Y. Bao, S. Chakravarthy, U. M. Muthurajan, K. Luger, Reconstitution of nucleosome core particles from recombinant histones and DNA. *Methods Enzymol.* **375**, 23–44 (2003). Medline doi:10.1016/S0076-6879(03)75002-2

18. J. R. Lakowicz, *Principles of Fluorescence Spectroscopy* (Springer, Berlin, 2007).

19. M. Richter, A. Chakrabarti, I. R. Ruttekolk, B. Wiesner, M. Beyermann, R. Brock, J. Rademann, Multivalent design of apoptosis-inducing bid-BH3 peptide-oligosaccharides boosts the intracellular activity at identical overall peptide concentrations. *Chem. Weinh. Bergstr. Ger.* **18**, 16708–16715 (2012). Medline doi:10.1002/chem.201202276

20. T. Nguyen, M. B. Francis, Practical synthetic route to functionalized rhodamine dyes. *Org. Lett.* **5**, 3245–3248 (2003). Medline doi:10.1021/ol035135z

21. E. Kassianidis, R. J. Pearson, D. Philp, Probing structural effects on replication efficiency through comparative analyses of families of potential self-replicators. *Chem. Weinh. Bergstr. Ger.* **12**, 8798–8812 (2006). Medline doi:10.1002/chem.200600460

22. T. Forster, Energiewanderung und fluoreszenz. *Naturwissenschaften* **33**, 166–175 (1946). doi:10.1007/BF00585226

23. M. Lorenz, A. Hillisch, S. D. Goodman, S. Diekmann, Global structure similarities of intact and nicked DNA complexed with IHF measured in solution by fluorescence resonance energy transfer. *Nucleic Acids Res.* **27**, 4619–4625 (1999). Medline doi:10.1093/nar/27.23.4619

24. L. Stryer, R. P. Haugland, Energy transfer: A spectroscopic ruler. *Proc. Natl. Acad. Sci. U.S.A.* **58**, 719–726 (1967). Medline doi:10.1073/pnas.58.2.719

25. G. A. Crosby, J. N. Demas, Measurement of photoluminescence quantum yields. *J. Phys. Chem.* **75**, 991–1024 (1971) Review. doi:10.1021/j100678a001

26. R. F. Kubin, A. N. Fletcher, Fluorescence quantum yields of some rhodamine dyes. *J. Lumin.* **27**, 455–462 (1982). doi:10.1016/0022-2313(82)90045-X

27. Z.-Y. Kan, L. Mayne, P. S. Chetty, S. W. Englander, ExMS: Data analysis for HX-MS experiments. *J. Am. Soc. Mass Spectrom.* **22**, 1906–1915 (2011). Medline doi:10.1007/s13361-011-0236-3

28. S. R. Kline, Reduction and analysis of SANS and USANS data using IGOR Pro. *J. Appl. Cryst.* **39**, 895–900 (2006). doi:10.1107/S0021889806035059

29. A. E. Whitten, S. Cai, J. Trewhella, *MULCh* : Modules for the analysis of small-angle neutron contrast variation data from biomolecular assemblies. *J. Appl. Cryst.* **41**, 222–226 (2008).

30. B. E. Black, L. E. Jansen, P. S. Maddox, D. R. Foltz, A. B. Desai, J. V. Shah, D. W. Cleveland, Centromere identity maintained by nucleosomes assembled with histone H3 containing the CENP-A targeting domain. *Mol. Cell* **25**, 309–322 (2007). Medline doi:10.1016/j.molcel.2006.12.018

31. D. Ray-Gallet, A. Woolfe, I. Vassias, C. Pellentz, N. Lacoste, A. Puri, D. C. Schultz, N. A. Pchelintsev, P. D. Adams, L. E. Jansen, G. Almouzni, Dynamics of histone H3 deposition in vivo reveal a nucleosome gap-filling mechanism for H3.3 to maintain chromatin integrity. *Mol. Cell* **44**, 928–941 (2011). Medline doi:10.1016/j.molcel.2011.12.006

32. P. Khandelia, K. Yap, E. V. Makeyev, Streamlined platform for short hairpin RNA interference and transgenesis in cultured mammalian cells. *Proc. Natl. Acad. Sci. U.S.A.* **108**, 12799–12804 (2011). Medline doi:10.1073/pnas.1103532108

33. E. A. Bassett, S. Wood, K. J. Salimian, S. Ajith, D. R. Foltz, B. E. Black, Epigenetic centromere specification directs aurora B accumulation but is insufficient to efficiently correct mitotic errors. *J. Cell Biol.* **190**, 177–185 (2010). Medline doi:10.1083/jcb.201001035

34. C. A. Schneider, W. S. Rasband, K. W. Eliceiri, NIH Image to ImageJ: 25 years of image analysis. *Nat. Methods* **9**, 671–675 (2012). Medline doi:10.1038/nmeth.2089

35. M. Hall, E. Frank, G. Holmes, B. Pfahringer, P. Reutemann, I. H. Witten, The WEKA data mining software: An update. *SIGKDD Explor. Newsl.* **11**, 10–18 (2009). doi:10.1145/1656274.1656278

36. D. Pelleg, A. Moore, in *Proceedings of the 17th International Conf. on Machine Learning* (Morgan Kaufmann, San Francisco, 2000), pp. 727–734.

37. D. L. Bodor, M. G. Rodríguez, N. Moreno, L. E. T. Jansen, Analysis of protein turnover by quantitative SNAP-based pulse-chase imaging. *Curr. Protoc. Cell Biol.* (Juan Bonifacino), Chapter 8, Unit8.8 (2012).

38. P. Heun, S. Erhardt, M. D. Blower, S. Weiss, A. D. Skora, G. H. Karpen, Mislocalization of the *Drosophila* centromere-specific histone CID promotes formation of functional ectopic kinetochores. *Dev. Cell* **10**, 303–315 (2006). Medline doi:10.1016/j.devcel.2006.01.014

39. N. Lacoste, A. Woolfe, H. Tachiwana, A. V. Garea, T. Barth, S. Cantaloube, H. Kurumizaka, A. Imhof, G. Almouzni, Mislocalization of the centromeric histone variant CenH3/CENP-A in human cells depends on the chaperone DAXX. *Mol. Cell* **53**, 631–644 (2014). Medline doi:10.1016/j.molcel.2014.01.018

40. S. W. Englander, Hydrogen exchange and mass spectrometry: A historical perspective. *J. Am. Soc. Mass Spectrom.* **17**, 1481–1489 (2006). Medline doi:10.1016/j.jasms.2006.06.006

41. R. D. Shelby, K. Monier, K. F. Sullivan, Chromatin assembly at kinetochores is uncoupled from DNA replication. *J. Cell Biol.* **151**, 1113–1118 (2000). Medline doi:10.1083/jcb.151.5.1113

42. Y. Bai, J. S. Milne, L. Mayne, S. W. Englander, Primary structure effects on peptide group hydrogen exchange. *Proteins* **17**, 75–86 (1993). Medline doi:10.1002/prot.340170110

43. P. Hemmerich, S. Weidtkamp-Peters, C. Hoischen, L. Schmiedeberg, I. Erliandri, S. Diekmann, Dynamics of inner kinetochore assembly and maintenance in living cells. *J. Cell Biol.* **180**, 1101–1114 (2008). Medline doi:10.1083/jcb.200710052

44. T. Fukagawa, W. R. Brown, Efficient conditional mutation of the vertebrate CENP-C gene. *Hum. Mol. Genet.* **6**, 2301–2308 (1997). Medline doi:10.1093/hmg/6.13.2301

45. D. R. Foltz, L. E. Jansen, A. O. Bailey, J. R. Yates 3rd, E. A. Bassett, S. Wood, B. E. Black, D. W. Cleveland, Centromere-specific assembly of CENP-a nucleosomes is mediated by HJURP. *Cell* **137**, 472–484 (2009). Medline doi:10.1016/j.cell.2009.02.039

46. D. Liu, M. Vleugel, C. B. Backer, T. Hori, T. Fukagawa, I. M. Cheeseman, M. A. Lampson, Regulated targeting of protein phosphatase 1 to the outer kinetochore by KNL1 opposes Aurora B kinase. *J. Cell Biol.* **188**, 809–820 (2010). Medline doi:10.1083/jcb.201001006

47. T. Furuyama, C. A. Codomo, S. Henikoff, Reconstitution of hemisomes on budding yeast centromeric DNA. *Nucleic Acids Res.* **41**, 5769–5783 (2013). Medline doi:10.1093/nar/gkt314

48. M. Bui, E. K. Dimitriadis, C. Hoischen, E. An, D. Quénet, S. Giebe, A. Nita-Lazar, S. Diekmann, Y. Dalal, Cell-cycle-dependent structural transitions in the human CENP-A nucleosome in vivo. *Cell* **150**, 317–326 (2012). Medline doi:10.1016/j.cell.2012.05.035

49. S. Henikoff, S. Ramachandran, K. Krassovsky, T. D. Bryson, C. A. Codomo, K. Brogaard, J. Widom, J. P. Wang, J. G. Henikoff, The budding yeast Centromere DNA Element II wraps a stable Cse4 hemisome in either orientation in vivo. *eLife* **3**, e01861 (2014). Medline doi:10.7554/eLife.01861

50. A. Guse, C. W. Carroll, B. Moree, C. J. Fuller, A. F. Straight, In vitro centromere and kinetochore assembly on defined chromatin templates. *Nature* **477**, 354–358 (2011). Medline doi:10.1038/nature10379

51. M. R. Przewloka, Z. Venkei, V. M. Bolanos-Garcia, J. Debski, M. Dadlez, D. M. Glover, CENP-C is a structural platform for kinetochore assembly. *Curr. Biol.* **21**, 399–405 (2011). Medline doi:10.1016/j.cub.2011.02.005

52. E. Screpanti, A. De Antoni, G. M. Alushin, A. Petrovic, T. Melis, E. Nogales, A. Musacchio, Direct binding of Cenp-C to the Mis12 complex joins the inner and outer kinetochore. *Curr. Biol.* **21**, 391–398 (2011). Medline doi:10.1016/j.cub.2010.12.039

53. J. Tomkiel, C. A. Cooke, H. Saitoh, R. L. Bernat, W. C. Earnshaw, CENP-C is required for maintaining proper kinetochore size and for a timely transition to anaphase. *J. Cell Biol.* **125**, 531–545 (1994). Medline doi:10.1083/jcb.125.3.531

54. K.-J. Armache, J. D. Garlick, D. Canzio, G. J. Narlikar, R. E. Kingston, Structural basis of silencing: Sir3 BAH domain in complex with a nucleosome at 3.0 Å resolution. *Science* **334**, 977–982 (2011). Medline doi:10.1126/science.1210915

55. R. D. Makde, J. R. England, H. P. Yennawar, S. Tan, Structure of RCC1 chromatin factor bound to the nucleosome core particle. *Nature* **467**, 562–566 (2010). Medline doi:10.1038/nature09321

56. J. F. Pardon, D. L. Worcester, J. C. Wooley, K. Tatchell, K. E. Van Holde, B. M. Richards, Low-angle neutron scattering from chromatin subunit particles. *Nucleic Acids Res.* **2**, 2163–2176 (1975). Medline doi:10.1093/nar/2.11.2163